NTNU
Norwegian University of
Science and Technology

Prelimenary preprocessing of ECG-signals for use in multivariate analysis

Mikael Dyb Wedeld

Master of Science in Cybernetics and Robotics
Submission date: June 2018
Supervisor: Harald Martens, ITK
Co-supervisor: Nils Kristian Skjærvold, St. Olavs Hospital

Norwegian University of Science and Technology
Department of Engineering Cybernetics

preface

This master's thesis in signal processing of ECG-signals was done at NTNU as part of the Engineering Cybernetics program. The thesis was done during Spring 2018, and the idea for this thesis was inspired by supervisor Harald Martens, who proposed the initial idea for heart modeling based on multivariate principles. During the thesis, much of the physiological information that helped form the methods was provided by co-supervisor Nils Kristian Skjærsvold. Feedback on the content and layout of the thesis was provided by Nils Kristian Skjærsvold, and also by Ph.D. student Silje S.Fuglerud. The main programming language used in the thesis was MATLAB R2017b by MathWorks, and the thesis was written in the Overleaf LaTeX editor. The instruments for the ECG measurements was provided by St. Olavs Hospital and consisted of a Bio Amp FE132, a three-pack of Shielded Lead Wires MLA2503, and a 3 Lead Shielded Bio Amp Cable MLA2340 from ADinstruments. Fellow student Tina Danielsen worked with some of the challenges on Blood Pressure signals, and several methods in the thesis were refined after discussion with her. An interested reader is advised to have a solid understanding of Fourier Transforms and Convolution, with some rudimentary knowledge of digital filters and adaptive algorithms.

Trondheim, 2018-06-1

Mikael Dyb Wedeld

Summary

In order lay the framework for a possible multivariate heart model, a set of methods for preprocessing an electrocardiogram signal has been created. A normalized least mean square adaptive filter was created for filtering out high-frequency noise and power line interference, and the baseline wandering was estimated using respectively a Savitzky-Golay smoothing filter, a Discrete Wavelet Transform, and an Empirical Mode Decomposition, with the Discrete Wavelet Transform showing most promise out of the three. The separate heart cycles in the signal were accurately identified using another Discrete Wavelet Transform, and an algorithm was implemented for splitting the signal and arranging the cycles on top of each other. A method for classifying cycles that showed abnormal behaviour was created, which captured all artifacts, but will be in need of further tuning. An estimation of the respiratory rate was also done, and the frequency content could be observed in the power spectrum of the heart rate variability.

Sammendrag

For å legge grunnlaget for en mulig multivariat hjertemodell, har et sett med metoder for pre-prosessering av elektrokardiogram signaler blitt laget. et normalisert minste kvadraters adaptivt filter ble laget for å filtrere ut høyfrekvent støy og strømnettforstyrrelser, og grunnlinjebevegelsene ble estimert gjennom henholdsvis et Savitzky-Golay jevningsfilter, en diskret wavelet transformasjon, og en empirisk tilstandsdekomposisjon (Empirical Mode Decomposition), hvor den diskret wavelet transformasjonen presterte best ut av de tre. De individuelle hjerteslagene i signalet ble nøyaktig identifisert gjennom bruk av en ytterliger diskret wavelet transformasjon, og en algoritme ble implementert for å splitte signalet og arrangere slagene oppå hverandre. En metode for å klassifisere slag som viste unormal oppførsel ble prøvd, og som klarte å fange alle artifakter, men vil trenge ytterligere arbeid. En estimering av respirasjonsraten ble også gjort, og frekvensinnholdet kunne bli observert i energispekteret (power spectrum) til pulsvariabiliteten (heart rate variability).

Acknowledgements

I would like to thank the following persons for their great help during this master's thesis. First of all, my supervisor Harald Martens. A man with more belief in the ability of his students I've yet to meet, and his everlasting optimism and support have greatly inspired me, both in writing this thesis and in working on the challenges yet to come. My co-supervisor Nils Kristian Skjærsvold, for providing me with a physiological and practical point of view in this thesis. Without his valuable advise, the thesis would have been a lot more abstract than it is now. My fellow student Tina Danielsen, who have worked on many of the same problems as me and has an uncanny ability to see solutions to seemingly impossible problems. I am most grateful for her help. Silje S.Fuglerud, for being ever helpful and available despite her own considerable workload. Her constructive feedback has been very appreciated, and has resulted in a vastly improved layout for this thesis.

Abbrivations

CWT	Continuous Wavelet Transform
DWT	Discrete Wavelet Transform
ECG	Electrocardiography
EDR	ECG derived respiration
EMD	Empirical Mode Decomposition
FIR	Finite Impulse Response
HRV	Heart Rate Variability
IIR	Infinite Impulse Response
IMF	Intrinsic Mode Functions
MODWT	Maximum Overlap Discrete Wavelet Transform
MSE	Mean Square Error
NLMS	Normalized Least Mean Square
PAV	Peak Amplitude Variation
PLI	Power Line Interference
QRS	The three points on the ECG-signal that make up the characteristic peak caused by the heart contracting

Contents

Chapter 1

Introduction

1.1 Background

Problem Formulation

The introduction of the electrocardiograph gave medical personnel worldwide an invaluable tool for heart diagnostics, making it possible for them to view the hearts condition from a whole new perspective, where heart phenomena such as ectopic beats or myocardial infarctions could be easily discerned. Electrocardiography is, however, a very sensitive method of measuring, and the signal received can easily be corrupted by known sources of noise such as power line interference(PLI), baseline wandering due to respiration, and stochastic noise due to activity in the muscles(muscle noise). Some of these can be separated from the signal without much trouble, but others, and especially muscle noise, can have a frequency content that is deeply intertwined with that of the actual heart activity, making it hard to process without changing the desired information content. Additionally, practitioners of ECG today are primarily concerned with local time events in the heart, that is, they look at what is happening in the heart at the time of measurement, and they often apply the same method of analysis to all their patients, making observations and decisions based on a standardized set of rules for ECG-data. Though this still yields a lot of useful information, they will, in doing so, miss two great opportunities. First of all, observing the heart over a short window of time might not give enough information to predict the hearts condition, and if one uses an approach based on multivariate principles, it can be possible to consider the heart in a long-term perspective, in which it is quite simple to tell, from very minute changes, when the heart is starting behave "abnormally". Secondly, every individual is uniquely different, heart included, and taking this into consideration when making an ECG-diagnosis makes for a data-driven approach, where a potential model for determining the state of a subject's heart can make decisions based on what is considered normal for that patient. Thus, there is room and need for a set of methods that can take in an ECG-signal, preferably in real-time, and treat it in a way that filters out the parts that are guaranteed noise, extracts and keeps the parts that are undesired (but still might contain useful physiological information), and arrange the processed signal on a multivariable form that is easy for the practitioner to interpret. This thesis shall therefore attempt to create such a set of methods, with the multivariate approach being primarily concerned with changes in the morphology of the individual heartbeats. For now, this will only be done on static data, but in way that ideally can be easily extended to a real-time scenario.

Related work

On the topic of filtering the ECG-signal, extensive research has been done from a wide set of perspectives and approaches, and it is not feasible to account for them all. Of the ones that have worked on topics strongly related to this thesis, there are Manosueb, Jeerasuda & Paramote [4] who uses an adaptive filter in order to remove the Power Line Interference(PLI). By expressing the PLI as a sum of a sine wave and a cosine wave, and by proposing a method for calculating the optimal initial weight of the filter, they reduce both the Mean Square Error(MSE) and improve the Signal to Noise Ratio(SNR). A more general approach to ECG filtering using adaptive filters, where baseline wandering, muscle noise, and motion artifacts are considered in addition to the PLI, have been done by Thakor & Zhu [21]. They present several adaptive filter structures such as the Least-Mean-Squares(LMS) algorithm and the Adaptive Recurrent Filter, and how they can be implemented not only for noise cancellation but also for arrhythmia and ectopic heartbeats. Both of these builds again upon the principles set forth by Widrow, Glover & McCool [6], who showed the strength of using adaptive filters for noise canceling in such data as, for example, ECG signals. On ECG filtering using wavelet transforms, Addison [3] has done an extensive paper on the subject, not only in-depth explaining how both Continuous and Discrete Wavelet Transform (CWT & DWT) might be used for noise cancellation and baseline adjustment, but also thoroughly describes how they can be applied in order to solve a wide range of medical challenges such as robust QRS-identification, arrhythmia detection etc. Furthermore, on the topic of identifying and detecting R-peaks, a recent study by Park, Lee & Park [16] has used a combination of DWT and Modified Shannon energy envelope in order to detect the R-peak in the 48 first-channel ECG records from the MIT-BIH arrhythmia database, obtaining an accuracy of 99.84%. Other similar studies that use WT in order to detect R-peaks, are as mentioned Addison [3], Rabbani et al. [14], who combine WT and the Hilbert Transform for R-detection in highly noisy environments, and Merah et al. [18], who uses an approach based on the Stationary Wavelet Transform (also known as Dyadic wavelet transform, or Maximum Overlap DWT). Regarding the challenge of ECG baseline wandering removal, Jayant et al. [5] gives a compact overview over different existing techniques together with some of their strengths and weaknesses. Several of these techniques are tried by Lenis et al. [12] a attempt to minimize the artificial change in the ST-segment so that any diagnosis of ischemia or infarction is as accurately as possible. On their simulated 500 Hz ECG-signals, They found that the wavelet-based baseline cancellation performed best out of the methods, but that an almost equally good result could be obtained with a computationally much faster butterworth filter. Other attempts to solve the problem has been, amongst others, tried by Rastogi and Mehra [20] who combines the use of a Savitzky-Golay filter and a Daubechies (db4) wavelet. An approach using multivariate Empirical Mode Decomposition and Hilbert vibration decomposition [32] was used by Gupta et al. [25], who evaluated the method by adding ECG baseline signals, gathered from the MIT-BIH noise stress test database, on synthetically and measured ECG-signals before testing. They found the baseline wandering to be accurately represented by the last two IMFs, and obtained good results by simple extraction of these from the ECG-signal. Regarding identification and estimation of the ECG derived respiration (EDR), Moody et al. [11] found the respiratory rate by observing the changes in the mean cardiac electrical axis direction caused by expansion and contraction of the chest. By interpolating these axises with cubic spline, they found significant resemblance to the respiratory signal found using a pneumatic respiration transducer. Sarkar, Bhattacherjee and Pal [29] compared the respiration rate derived from respectively Heart Rate Variability (HRV) and Peak Amplitude Variation (PAV), and used both synthetic and real-time data. In both, they found that HVR performs overall better than PAV. To the authors knowledge, no papers on individual focused multivariate heart modeling exists that is strongly related to the approach used in this thesis.

What Remains to be Done?

Though a lot of work has been done on noise cancellation and baseline wandering removal, there are still room for improvement. Many of the papers done on these subjects concerns themselves primarily with either synthetic data, or measurements done under ideal circumstances. Therefore, though they might show great results for that specific situation, little evidence exists that tells whether or not they would perform well in other environments, and to the authors knowledge, robustness has been a little focused area of ECG-signal treatment methods.

1.2 Objectives

The main objectives of this Master's project are as follows

1. Remove or significantly reduce the high-frequency noise in the ECG-signal by implementing a Normalized Least Mean Square filter.
2. Estimate and extract the baseline wandering and baseline shifts from the signal by using a Savitzky-Golay filter, a Discrete Wavelet Transform, and an Empirical Mode Decomposition.
3. Implement an algorithm for detecting QRS-complexes and estimating the heart rate.
4. Create an algorithm for separating the heartbeats, classifying them as either "normal" or artifacts, and arrange them into separate matrices respectively on top of each other.
5. Attempt to identify the respiration rate and respiration form from the ECG-signal by observing the frequency content contained in the HRV.

1.3 Approach

First of all, the previously implemented low-pass filter from the project work shall be improved upon in order to attempt removing/reducing the ringing artifacts (Fig:1.1)

combining this with a wish for making the filter robust against both power line interference (PLI) and stochastic noise, a Normalized Least Mean Square (NLMS) filter shall be implemented and tuned. As the desired signal input to this filter, a FIR filtered version of the ECG-signal with an added 50 Hz sine wave noise shall be used. The filter will then be tested on ECG-measurements taken from 7 different subjects. Next, the baseline wandering and baseline shifts shall be estimated, singled out from the rest of the signal, and extracted and kept for later analysis. This will not be attempted with a standard high-pass filter, and among the methods to be tested and compared to each other are a Savitsky-Golay smoothing filter, low-frequency removal by Empirical Mode Decomposition(EMD), and low-frequency removal

Figure 1.1: Low-pass filtered ECG-signal using a butterworth filter. Powerful and unwanted ringing artifacts can be seen after each R-peak

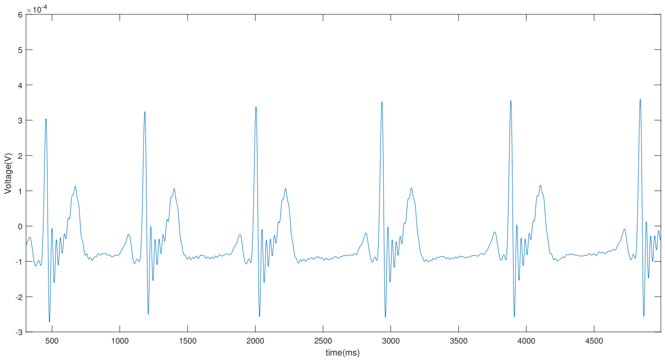

by Discrete Wavelet Transform(DWT). Further, a DWT will be done on the post-NLMS filtered signal, and the QRS-complexes shall be identified using peak detection on the transform plot of the DWT coefficients that is found to most closely correspond to the frequency range for QRS-complexes (approx. 0 Hz-20 Hz [17]). The resulting QRS-locations will then be used as anchor points for splitting the signal into separate cycles, and also for deciding the temporal and mean heart rate. Next, the signal separation distance shall be be adjusted to each separate subject based on their mean heart rate, and all the split cycles shall be arranged consecutively on top of each other in a matrix. As part of the artifact classification, this signal separation algorithm shall also create and set aside artifact cycles whenever a certain time passes without a new QRS-complex being detected. A second part of the artifact classification shall then be created, which will first create a reference cycle on some subset of already classified cycles, and then classify all new cycles by cross-correlation. This algorithm shall also be implemented so as to continuously update this reference cycle as new cycles are being processed. Lastly, the EDR shall be attempted estimated by straightforward power spectrum analysis of the HRV found in the QRS-complex procedure.

1.4 Limitations

The by far largest inconvenience during this project was the lack of actual respiratory measurements from the different subjects. A respiratory belt was provided during the measuring process, which measures the respiration using small piezo-electric elements that register the change in circumference around the thorax due to inhalation and exhalation. Unfortunately, the belt had a defect, and so no direct respiratory data could be recorded. This, in turn, made determining the accuracy of the different respiratory estimates found in this thesis difficult, as there was no reference respiration to compare them with. Though established methods of measuring respiration have been shown to give some small error [9], it would nonetheless have been quite illuminating to have this respiration data in order to provide some statistical insight on how successful this project had been in achieving the aforementioned objective. Furthermore, the quality of the measurements used for this project has been a subject of discussion. These are the same measurements that were recorded and used in the in-depth project leading up to this thesis, and briefly explained, the measurements were done by the author and his partner, both lacking any medical training, and therefore most likely resulting in above averagely noisy data[1]. In addition, the high sampling frequency of the instruments made some of the frequency bands, especially in the lower spectra, hard to discern. For the purpose of determining the accuracy of the different QRS-detection methods, it would also have helped to have someone with medical knowledge mark the QRS-complexes beforehand, so it would be possible to quantify the performance of the methods (e.g. as a percentage), though admittedly, the post-filtered signals were for the most part of high enough quality that an untrained eye could rather easily determine the position of an R-peak. This limitation is also extended to the baseline estimation in the sense that there were no reference baseline that one could compare the estimates to, so there was no way of accurately determine their accuracy other than empirically compare them to the signal. In addition, the methods have not been tested extensively on a larger samples size of diverse individuals. The 7 subjects the measurements were done on was healthy adults in the same age group (22-25 years old), and in order to see if the methods indeed detect known heart abnormalities (or on other age groups for that matter), testing should also have been done on data from patients with known cardiovascular diseases, or on geriatric patients.

---

[1] However, taking into consideration that the methods created in this thesis ideally should work on a wide range of different ECG-signals, one could argue that the heightened noise in the measurements actually helps the methods becoming more robust.

Chapter 2

Theory

2.1 Electrocardiography(ECG)

Electrocardiography(ECG) is the process of recording the electrical activity of the heart. This is done by using a set of electrodes placed on the skin that measures the minute electrical changes caused by the currents propagating through the tissue out from the heart. This is then shown on a connected monitor or printed out as seen in figure 2.4.

Figure 2.1: A 12-lead ECG of a healthy adult

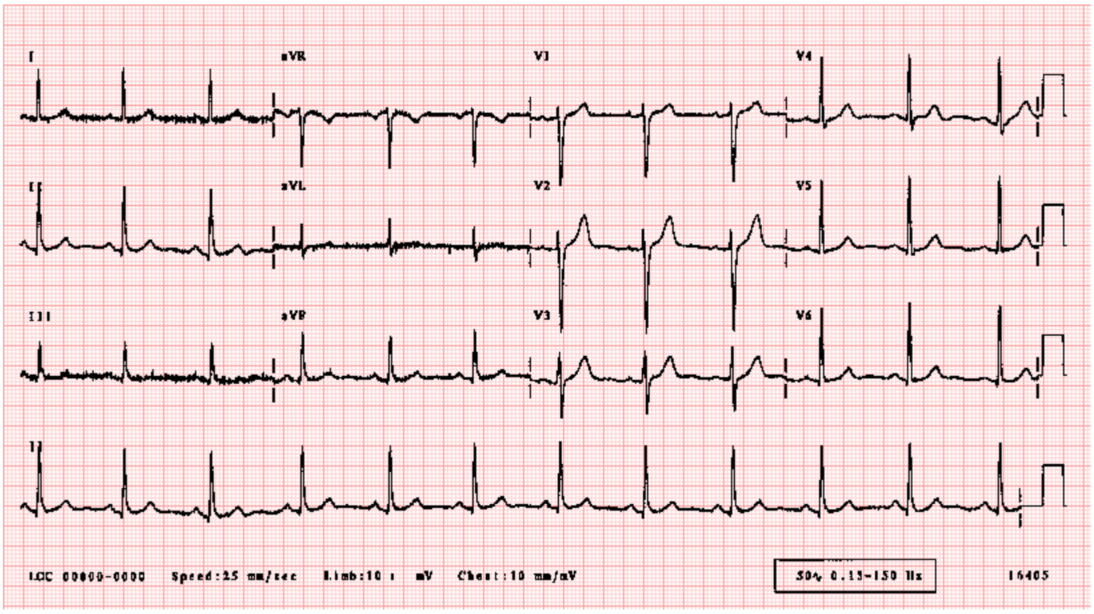

By placing as many as 4 leads on the limbs, and 6 leads across the chest, one can observe the heart from 12 different angles (or leads), which corresponds to the labels aVR, V1, V2 etc. in Figure 2.4. The most basic setup, and the one used for the data in this thesis consists of 3 leads on the right arm, left arm, and the left leg as shown in Figure 2.2a.

Figure 2.2: 3-lead ECG

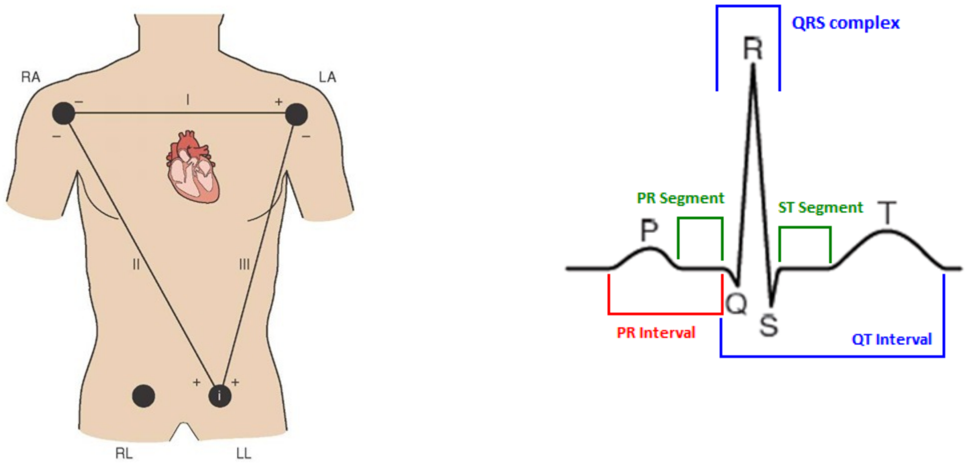

(a) The electrode placement in a 3-lead ECG setup.

(b) The electrode placement in a 3-lead ECG setup.

Measuring only the voltage directly across the heart along lead I, yields the most studied and known wave form Fig:2.2b, and many of the hearts primary functions can be easily observed here. Physiologically, and overly simplified, the different components in Fig:2.2b are as follows [38]:

- The P-wave represents the atrial depolarization or atrial contraction, that is responsible for filling the last approximately 30% of the ventricles before ventricular contraction. A large or irregular P-wave may indicate enlarged atria or nerve impulses coming from different sites.
- The QRS-complex represents the ventricular depolarization, or ventricular contraction that pushes the blood from the ventricles out in the body. Deep or wide QRS-complexes can indicate a possible myocardial infarction (heart attack) or other pathology.
- The T-wave represents the ventricular repolarization or relaxation of the cardiac muscles in the ventricles whereupon they enter a recovery period. Tall or peaked T-wave may indicate myocardial injuries.

2.2 Filtering techniques

As mentioned earlier, the ECG-signal is prone to several known sources of noise such as power line interference(PLI), baseline movement due to respiration, and muscle noise [31]. These sources of noise drastically change the signal form, and since much of the desired information in the signal is derived directly from it morphology, some sort filtering technique was necessary in order to glean this information. A short presentation will therefore be made here of different classes of filters tried on the signals, their mathematical construction, and their strength and weaknesses. The section on the Least-Mean-Square algorithm is heavily based on the book by Haykin about Neural Networks [13]

2.2.1 Finite impulse response filters

Finite impulse response filters or FIR filters is a class of digital filters which have, as the name implies, finite impulse response. That is, when subject to an impulse (e.g. a Kronecker delta function), every value of that filters response for $t \to \infty$ will be zero. When looking at the transfer function for the general digital filter of arbitrary order N [34]

$$\frac{y_n}{x_n} = \frac{\sum_{i=0}^{N} a_i z^{-i}}{\sum_{i=0}^{N} b_i z^{-i}}, \tag{2.1}$$

where y_n and x_n is the respective output and input, a_i is the feedforward filter coefficients, b_i is the feedback filter coefficients, and z^{-i} is the the delay operator ($z^{-i}x_n = x_{n-i}$). We can see that the filters behavior is caused by the non-trivial nature of the denominator, but in the case of a FIR-filter, we usually set b_0 to 1, and all other values of b to 0. Thus, the filters response will not be dependent on earlier responses (due to zero feedback). One great advantage this gives, is that no FIR filter response can be unstable (again, due to zero feedback), and they will usually outperform IIR filters in terms of accuracy. IIR filters, however, will usually have a faster response time, and is overall easier to tune and implement.

2.2.2 Least mean square filter

Let us now assume that our signal is the sum of N different independent signals x, each with their own corresponding weight w, that is

$$y = \sum_{k=1}^{N} w_k x_k, \tag{2.2}$$

If we further assume some desired response signal d, the error between them will be defined as

$$e = d - y. \tag{2.3}$$

and as a cost function J for minimizing e, we introduce the mean square error(MSE)

$$J = \frac{1}{2}E[e^2], \tag{2.4}$$

The linear optimum filtering problem is thus to determine a set of weights w that minimizes J. The resulting filter is called a Wiener filter, after its creator Norbert Wiener [37], and by inserting Eq2.2 in Eq2.3 and Eq2.3 in Eq2.4, we can write the MSE as

$$J = -\frac{1}{2}E[d^2] - E[\sum_{k=1}^{n} w_k x_k d] + \frac{1}{2}E[\sum_{k=1}^{n}\sum_{j=1}^{n} w_k w_j x_k x_j], \tag{2.5}$$

which, by assuming constant weights, can be written as

$$J = -\frac{1}{2}E[d^2] - w_k \sum_{k=1}^{n} E[x_k d] + \frac{1}{2}w_k w_j \sum_{k=1}^{n}\sum_{j=1}^{n} E[x_k x_j], \tag{2.6}$$

We now have three different expectation terms, and define

$$r_d = E[d^2], \tag{2.7}$$

as the mean-square value of the desired response d,

$$r_{dx}(k) = E[x_k d], \tag{2.8}$$

as the cross-correlation function between x_k and d, and

$$r_x(j,k) = E[x_k x_j], \tag{2.9}$$

as the auto-correlation function of x itself. Inserting these into Eq2.6, we obtain

$$J = -\frac{1}{2}r_d - \sum_{k=1}^{n} w_k r_{dx}(k) + \frac{1}{2}\sum_{k=1}^{n}\sum_{j=1}^{n} w_k w_j r_x(j,k), \tag{2.10}$$

In order to minimize this cost function, we have to differentiate it with respect to w_k and set the result to zero for every k. This gives us the expression for the gradient of the filters error surface.

$$\nabla_w J = \frac{\partial J}{\partial w_k}, k = 1, 2, \ldots, p, \tag{2.11}$$

Inserting Eq2.10 into this gradient expression yields us

$$\nabla_w J = -r_{dx}(k) + \sum_{j=1}^{n} w_j r_x(j, k), \tag{2.12}$$

which by setting equal to zero gives us

$$\sum_{j=1}^{n} w_{oj} r_x(j, k) = r_{dx}(k), \quad k = 1, 2, \ldots, p. \tag{2.13}$$

This set of equations is called the Wiener-Hopf equations, where w_{oj} denotes the optimal weights of the aforementioned Wiener filter that solves these equations. One popular method for solving these equations is the method of steepest descent, in which the weights assumes a time-varying form that iteratively adjusts themselves along the error surface towards an optimal solution. The optimal solution will be at the bottom point of the error surface, and intuitively, one sees that the weights of the filter should be adjusted so that they point in the direction of steepest descent, which will be the opposite of the gradient vector given by Eq2.12.

Figure 2.3: The method of steepest descent for one weight

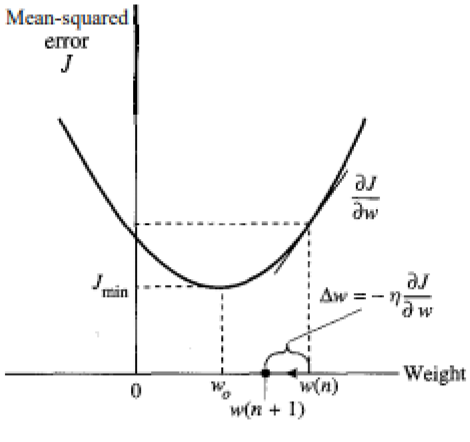

If we now let $w_k(n)$ be the weight at the iterative step n by the method of steepest descent, the corresponding filter equation 2.12 will also take on a time-varying iterative form

$$\nabla_w J(n) = -r_{dx}(k) + \sum_{j=1}^{n} w_j(n) r_x(j,k), \tag{2.14}$$

and for any step n, the adjustment applied to $w_k(n)$ as per method of steepest descent will be

$$\Delta w_k(n) = -\eta \nabla_{wk} J_n, \tag{2.15}$$

where η is the learning-rate parameter, or step size, which is a positive parameter that determines the speed and accuracy of error convergence. We can now formulate the expression for the value the updated weight $w-k(n+1)$ as

$$w_k(n+1) = w_k(n) + \Delta w_k(n) = w_k(n) - \eta \nabla_{wk} J_n, \tag{2.16}$$

and inserting Eq2.14 in Eq2.20 gives the method of steepest descent expressed in terms of the correlation functions $r_x(j,k)$ and $r_{dx}(j,k)$

$$w_k(n+1) = w_k(n) - \eta[r_{dx}(k) - \sum_{j=1}^{M} w_j(n) r_x(j,k)], \quad k = 1, 2, \ldots, p. \tag{2.17}$$

However, the method of steepest descent requires a priori knowledge about the signal x_k in order to calculate the spatial correlation functions $r_{dx}(k)$ and $r_x(j,k)$, which will not be available in the case where the filter must operate in unknown environments. In addition, one must take great care when choosing a step-size η, as both performance and accuracy are greatly decided by this. In order to compensate for this, we finally turn to the least-mean-square algorithm which is an approach that uses instantaneous estimates of $r_x(j,k)$ and $r_{dx}(j,k)$. These are defined directly from Eq2.8 as

$$\hat{r}_{dx}(k;n) = x_k(n) d(n), \tag{2.18}$$

and from Eq2.9 as

$$\hat{r}_x(j,k;n) = x_k(n) x_j(n), \tag{2.19}$$

We thus have transformed the expressions for cross-correlation and autocorrelation over in a non-stationary general form, where both the signals and the desired response has taken on time-varying forms. inserting Eq2.18 and Eq2.19 into Eq2.20, gives us the finalized expression for the computation of the weight estimates as

$$\begin{aligned}\hat{w_k}(n+1) &= \hat{w_k}(n) + \eta[x_k(n)d(n) - \sum_{j=1}^{P} \hat{w_j}(n)x_j(n)x_k(n)] \\ &= \hat{w_k}(n) + \eta[d(n) - \sum_{j=1}^{P} \hat{w_j}(n)x_j(n)]x_k(n) \\ &= \hat{w_k}(n)\eta[d(n) - y(n)]x_k(n), \quad k = 1, 2, \ldots, p.\end{aligned} \tag{2.20}$$

where $y(n)$ is the output of the spatial filter at iteration n, and $d(n) - y(n)$ is, as mentioned earlier, the error $e(n)$. Since the input $x_j(n)$ is sensitive to scaling, we'll also normalize the input in order to guarantee stability of the algorithm [13], and it is now simple to set up the normalized LMS algorithm as follows

Table 5.1 Summary of the NLMS algorithm

1.Initialization set

$\hat{w_k}(1) = 0$ **fork** $= 1, 2, \ldots, p$

2.Filtering. For time n= $1, 2, \ldots,$ **compute**

$y(n) = \sum_{j=1}^{p} \hat{w_j}(n)x_j(n)$

$e(n) = d(n) - y(n)$

$\hat{w_k}(n+1) = w_k(n) + \frac{\eta e(n)x_k(n)}{x^T x}$ **fork**$= 1, 2, \ldots, p$

A great advantage of this approach compared to the method of steepest descent is that it is instantaneous in the sense that it only seeks to minimize the instantaneous error squared, defined as $\frac{1}{2}e^2(n)$. The steepest method will try to minimize the sum of error squares integrated over all the previous iterations, thus needing to store this information for calculating the exact gradient vector, while the LMS algorithm will calculate a "random" gradient vector that will minimize the average error squared over time, only needing to store the information contained in the current weights of the filter. Since it can operate in non-stationary environments, it can also find an optimal solution when the minimum point of the error surface varies with time. On the flip-side, the stochastic behavior of the gradient vector also means that one often needs large sample sizes in order to achieve a small mean square error[1]. In addition, if the signal to be filtered is highly non-stationary, the tracking of the optimal solution will improve with smaller step-sizes η, but at the cost of a slower adaptation rate.

Figure 2.4: A schematic drawing of the principle idea behind an adaptive filter. The algorithm will update the weights of the linear FIR-filter based in the error e between the desired signal d and the output signal y

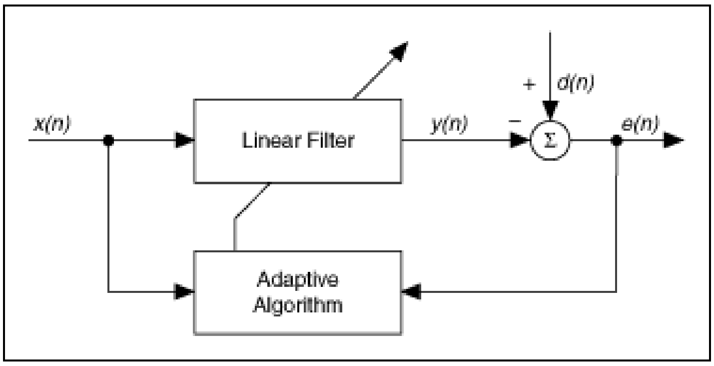

2.2.3 Savitzky-Golay filter

One of the simplest and most straightforward ways to smooth fluctuating data is to employ a moving average filter. For a point x_k in a discrete data set, and for a static number m, this can be thought of as summing all the points from x_{k-m} to x_{k+m} and dividing by the number of elements n contained in this interval. When this averaged value has been generated, one drops the last value x_{k-m}, adds a new value x_{k+m+1}, and repeats the process for the point x_{k+1}, that is

$$g_k = \sum_{i=k-m}^{k+m} C_i x_k, \tag{2.21}$$

where C_i is the filter coefficients with constant value $1/n$. This method works wonderfully as long as the underlying function that describes the data is constant or linear, but in the case of a non-zero second derivative, a bias will be introduced which will change the shape, and thereby information in the data [30]. In order to remove this highly undesirable trait, Savitzky and Golay proposed in 1964 a way of retaining the shape and form of the data while still using the principles of a moving window [1]. They sought to

---

[1] Unless one considers a large step-size η. However, one must in this cause be fairly certain of the statistics of the signal in order for the error rate to converge

replace the filter coefficients C_i with polynomials of higher order instead of the constant average. By least-square fitting this polynomial line to the n points inside the window, the smoothed value g_k would be chosen in such a way as to best retain the fundamental shape of the data (as seen in figure 2.5).

Figure 2.5: moving average filter (middle) and 4th order Savitzky-Golay filter (bottom) applied to a noisy chirp signal with window size 33. Notice how the moving average filter fails to retain the shape of the wave tops. [26]

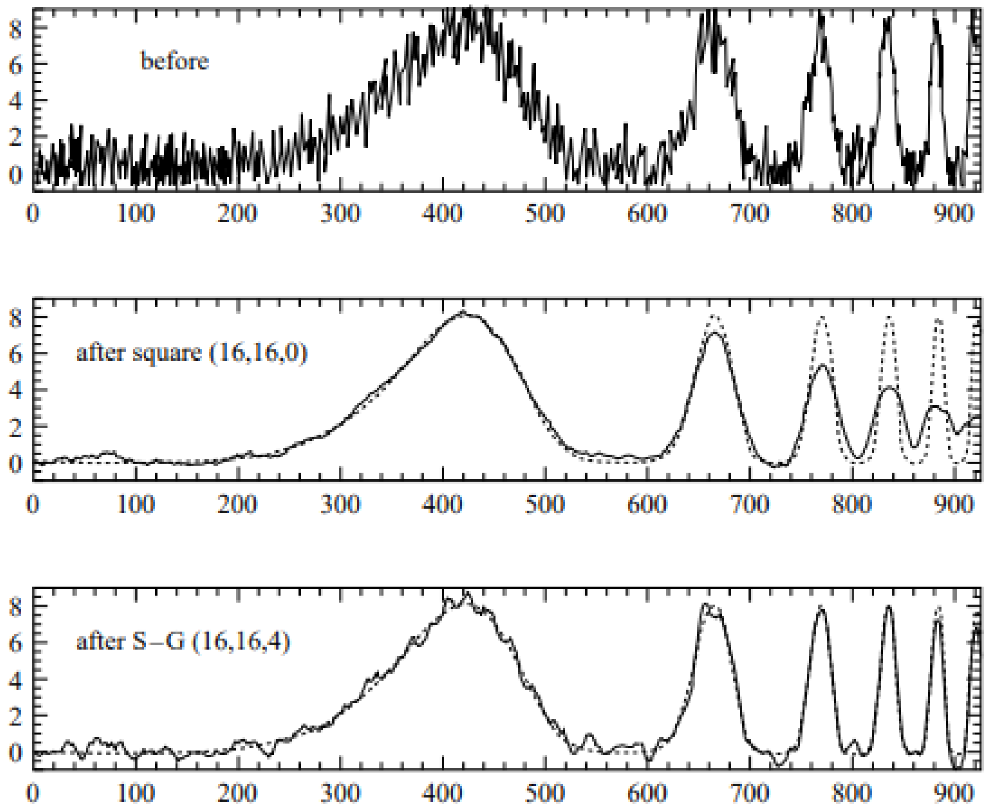

Mathematically, the problem is to find the best mean-square fit of a polynomial of degree p thorough the set of $2m+1$ consecutive values, where $p < 2m+1$, and the polynomial is on the form

$$g_k = \sum_{i=0}^{i=p} b_{pi} k^i = b_{p0} + b_{p1} k + b_{p2} k^2 + \ldots + b_{pi} k^p. \tag{2.22}$$

Taking the derivatives of this polynomial gives us

$$\frac{dg_k}{dk} = b_{p1} + 2b_{p2}k + 3b_{p3}k^2 + \ldots + pb_{pp}k^{p-1} \tag{2.23a}$$

$$\frac{d^2g_k}{dk^2} = 2b_{p2} + 6b_{p3}k + \ldots + (p-1)pb_{pp}k^{p-2} \tag{2.23b}$$

$$\frac{d^pg_k}{dk^p} = pb_{pp}. \tag{2.23c}$$

And since the least squares criterion requires us to minimize the sum of the squares of the differences between the observed values y_k and the estimated values g_k inside the window, we have that

$$\frac{\partial}{\partial b_{pi}}[\sum_{k=-m}^{k=m}(g_k - y_k)^2] = 0 \tag{2.24}$$

minimizing Eq2.24 with respect to b_{pk}, gives us

$$\begin{aligned} &\frac{\partial}{\partial b_{pk}}[\sum_{k=-m}^{k=m}(b_{p0} + b_{p1}k + \ldots + b_{pp}k^p - y_k)^2] \\ &= 2\sum_{k=-m}^{k=m}(b_{p0} + b_{p1}k + \ldots + b_{pp}k^p - y_k)k = 0 \end{aligned} \tag{2.25}$$

Since there are $n+1$ number of equations to calculate (one for each point of data), we can also minimize 2.24 with respect to the general b_{pr}, where r represents the index of the equation number, that is

$$\sum_{k=-m}^{k=m}[\sum_{i=0}^{i=p} b_{pi}k^i - y_k]k^r = 0, \tag{2.26}$$

which can be expressed as

$$\sum_{k=-m}^{k=m}\sum_{i=0}^{i=p} b_{pi}k^{i+r} = \sum_{k=-m}^{k=m} y_k k^r. \tag{2.27}$$

2.3 Detection of QRS-complexes

Next, not only for determining heart rate and R-peak magnitude but also for the purpose of later splitting the signal into separate heartbeats in order to compare them, a method for detecting individual QRS-complexes is necessary. Several methods and approaches have already been done on this subject [14]- [18], and this thesis will mostly use the Maximum Overlap Discrete Wavelet Transform (MODWT) for QRS-detection. The theory on wavelet transforms is based on the "Illustrated wavelet transform handbook" [2] by Addison.

2.3.1 Wavelets and the Discrete wavelet transform (DWT)

Wavelets are small "local" wavelike functions, and the principal idea behind their use in signal analysis is to convolute them with the signal in order to *transform* the signal over in a more useful form that better represents the signal information.

Figure 2.6: A set of different wavelets

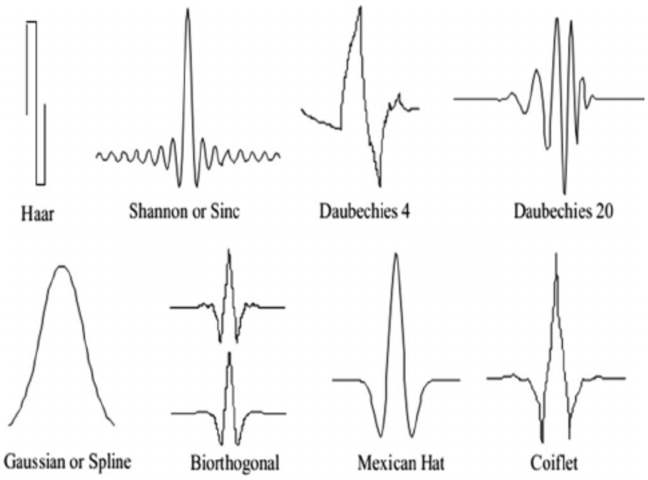

Mathematically, a wavelet has to satisfy certain criteria. If we denote the wavelet function as $\psi(t)$, then it must

1. Have finite energy

$$E = \int_{-\infty}^{\infty} |\psi(t)|^2 dt < \infty \tag{2.28}$$

2. If $\hat{\psi}(f)$ is the fourier transform of $\psi(t)$

$$\hat{\psi}(f) = \int_{-\infty}^{\infty} \psi(t) e^{-i(2\pi f)t} dt \tag{2.29}$$

then the following condition must hold

$$C_g = \int_{0}^{\infty} \frac{|\psi(f)|^2}{f} dt < \infty \tag{2.30}$$

where C_g is the *admissibility constant* that changes value depending on what wavelet form is used. These criteria simply mean that a wavelet must have a zero mean, and wavelets that fulfill the second condition operate in fact as bandpass filters, letting through frequencies contained in the bandpass defined by the wavelets corresponding energy spectrum. We will now consider a simple wavelet, the mexican hat wavelet (see Figure 2.6), defined as

$$\psi(t) = (1 - t^2) e^{(-t^2/2)} \tag{2.31}$$

When we convolute this wavelet with a signal $x(t)$, there are two operations we can do in order to manipulate the wavelet so it becomes more flexible for use in signal analysis. The first one is to stretch or compress (dilate) it, and the other one is to translate it along the time axis.

Figure 2.7: The two different wavelet manipulations, Dilation to the left (1), and translation to the right (2). [40]

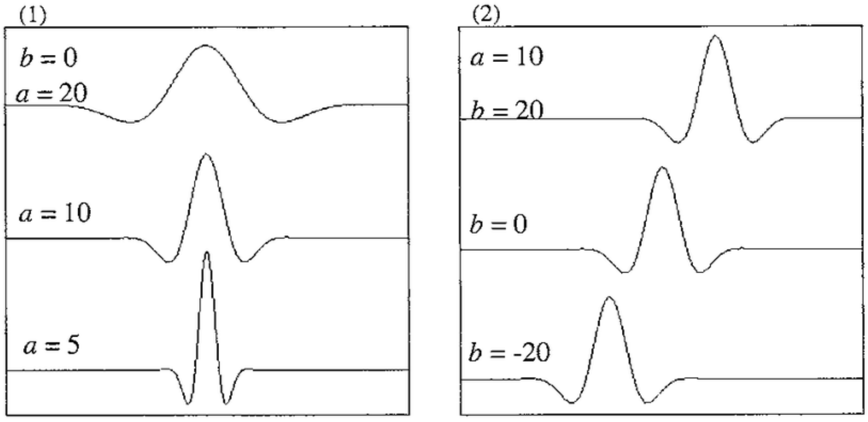

Denoting dilation and translation as the parameters a and b respectively, we can rewrite the mexican hat wavelet in this shifted and dilated version as

$$\psi(\frac{t-b}{a}) = [1 - (\frac{t-b}{a})^2] e^{-\frac{1}{2}[(t-b)/a]^2}. \tag{2.32}$$

The *wavelet transform* of a signal $x(t)$ with a wavelet $\psi(t)$ in the continuous case can now be defined as

$$T(a,b) = w(a)\int_{-\infty}^{\infty} x(t)\psi^*(\frac{t-b}{a})dt \tag{2.33}$$

Where $w(a)$ is the weighting function, and the asterisk tells us to use the complex conjugate of the wavelet transform if applicable (which is not the case for the mexican hat wavelet, or any other wavelet used throughout this thesis). For energy conservation purposes, $w(a) = 1/\sqrt{a}$ is often used (so that all scales of the wavelet have the same energy), and we can compactly write the normalized wavelet function as

$$\psi_{a,b} = \frac{1}{\sqrt{a}}\psi(\frac{t-b}{a}), \tag{2.34}$$

which in turn gives us the compact version of the continuous wavelet transform integral

$$T(a,b) = \int_{-\infty}^{\infty} x(t)\psi^*_{a,b}dt \tag{2.35}$$

We now see that the wavelet transform is simply a convolution of $x(t)$ and differently scaled versions of the wavelet that are slid along $x(t)$. If the wavelet at a certain scale a' has a high correlation with the signal at a certain position b', the corresponding transform value $T(a',b')$ will be high as well. Plotting a and b against each other can thus give us a clear view of whether or not patterns similar to the wavelet form exist somewhere in the signal, and can tell us how strongly they correlate with the signal, their temporal locations, and their approximate frequency contents. However, this also means that the quality of the analysis will depend largely on what wavelet is used, as one is restricted to a limited set of pre-existing wavelets. If you know a priori that your signal contains patterns that well fits one of the wavelets, you will obtain an accurate representation of that pattern using that wavelet. If the phenomena you're after does not match well any existing wavelet, you will, on the other hand, most likely not be able to discern the desirable information satisfactorily.

Now for the discrete case of the wavelet transform, we can no longer move continuously along the time axis but must move the wavelet in discrete steps, and also at discrete values of dilation. A natural choice for sampling the parameters a and b in Eq2.35 would be to logarithmically discretize the scale size a and then link it to the size of the step b. Thus, our movement

Figure 2.8: Signal showing yearly epidemiological occurrences. Two different scales of the wavelet are shown at the top with the signal, and at the bottom, we see clearly that the first wavelet scale captures the sine movement of the signal, while the other wavelet is too stretched out to correlate well with the signal. The plot is from a paper on spectral analysis on epidemiological time-series by Cazelles et al. [7]

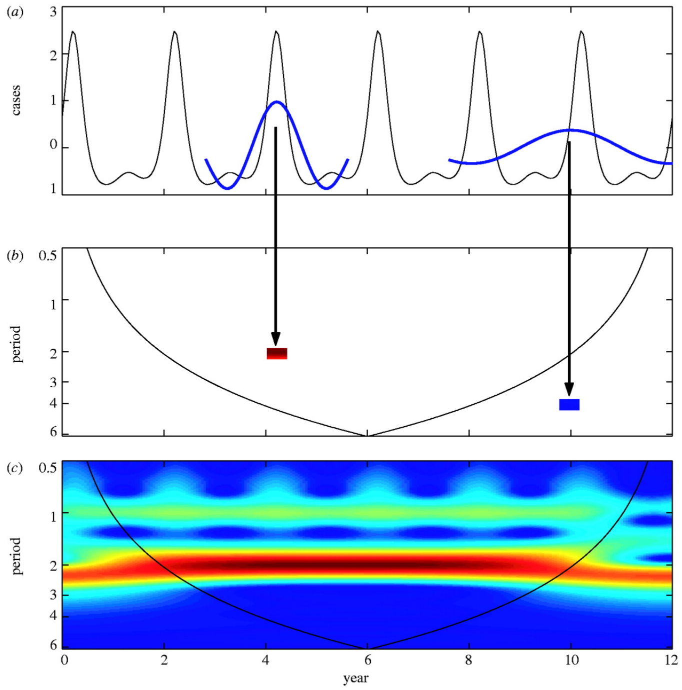

through time in steps of b is directly proportional to the scale a, and we can rewrite Eq2.35 in this form as

$$\psi_{m,n}(t) = \frac{1}{\sqrt{a_0^m}}\psi(\frac{t - nb_0a_0^m}{a_0^m}) \tag{2.36}$$

Where m and n are integers that control respectively wavelet dilation and wavelet translation, and which can be set to any real value. a_0 is a fixed dilation step parameter set to a value greater than 1, and b_0 is the location parameter set to any value greater than zero. Using this discrete wavelet form, we can now express the general discrete wavelet transform as

$$T_{m,n} = \int_{-\infty}^{\infty} x(t)\frac{1}{a_0^{m/2}}\psi(a_0^{-m}t - nb_0)dt \tag{2.37}$$

Where $T_{m,n}$ are known as the *detail coefficients*. One thing to watch out for is whether or not one might lose signal information in the transition from the continuous to the discrete transform. This is equal to asking whether or not one has lost energy, so by summing the energy of the detail coefficients, we can see if it lies within a certain bounded range of the energy E of the original signal, that is

$$AE \leq \sum_{m=-\infty}^{\infty} \sum_{n=-\infty}^{\infty} |T_{m,n}|^2 \leq BE \tag{2.38}$$

where ideally, A should be equal to B (that is, no information was lost in the transition). One easy and common way of conserving information, and that gives efficient discretization, is choosing a_0 and b_0 as 2 and 1 respectively. This power-of-two logarithmic scaling of both dilation and translation is known as the *dyadic grid* arrangement, and inserting $a_0 = 2$ and $b_0 = 1$ into Eq2.36 gives us the dyadic grid wavelet

$$\psi_{m,n}(t) = \frac{1}{\sqrt{2^m}}\psi(\frac{t - n2^m}{2^m}), \tag{2.39}$$

written more compactly as

$$\psi_{m,n}(t) = 2^{-m/2}\psi(2^{-m}t - n). \tag{2.40}$$

If we, in addition, normalize the dyadic grid wavelets, we will have an orthonormal wavelet basis, so that no information in any specific wavelet coefficient is repeated anywhere else, and so that all wavelet coefficients together completely define the original signal $x(t)$. Using the dyadic grid wavelet in 2.39, we can now express the *discrete wavelet transform*(DWT) as follows

$$T(m,n) = \int_{-\infty}^{\infty} x(t)\psi_{m,n}dt, \tag{2.41}$$

and the original signal $x(t)$ can be fully and completely reconstructed by doing the *inverse discrete wavelet transform*, which is simply the summation of the detail coefficients and the dyadic grid wavelet over all the wavelet translation and dilation parameters, that is

$$x(t) = \sum_{m=-\infty}^{\infty} \sum_{n=-\infty}^{\infty} T_{m,n}\psi_{m,n}(t). \tag{2.42}$$

2.4 Baseline and respiratory rate estimation

Finally, in order to estimate the baseline wandering, respiration form and respiration frequency, three methods were used. Savitzky-Golay as described earlier was used in baseline estimation, and DWT was used for both baseline and respiratory rate estimation. The final method was EMD, which will be briefly described here.

2.4.1 Empirical Mode Decomposition(EMD)

The Empirical Mode Decomposition is a technique for decomposing a signal into a set of functions called Intrinsic Mode Functions(IMFs). This technique is actually part of the Hilbert-Huang-Transform(HHT) [23], which is a method for observing the instantaneous frequency [22] in a data set, and EMD is a highly data-driven, a posteriori view of the time-frequency domain. This is due to how EMD only operates directly in the temporal space, treating the signal as is regardless of frequency content. However, for this approach to work, the assumption must be made that any signal consists of a finite number of oscillatory modes which is superimposed on top of each other [24], which often (due to the highly non-stationary nature of the real world) have widely different frequencies. These oscillatory modes are what is called IMFs, and there are two criteria that needs to be fulfilled in order for a function to qualify as an IMF, namely:

1. The number of extremum points and the number of zero-crossings in the data set must be equal, or at most differ by one.
2. The mean local value between the envelope defined by the maximum points, and the envelope defined by the minimum points, must be zero.

In order to construct these IMFs, EMD is implemented through a sifting process of the data set. This process will extract the modes in order from the highest frequencies to the lower ones, and the algorithm can be summarized as follows [36]:

1. identify all the local extrema in the data.
2. Create envelopes of respectively the upper and lower extrema by use of cubic spline lines.
3. Find the mean of the envelopes.
4. Use the difference between the data and the mean as a proto-IMF.
5. check the IMF criteria and a stoppage criterion in order to determine whether or not the proto-IMF qualifies as an IMF.

Figure 2.9: One step of the EMD sifting process. An upper and lower envelope has been created of the oscillatory signal, and the stippled line shows the mean. [35]

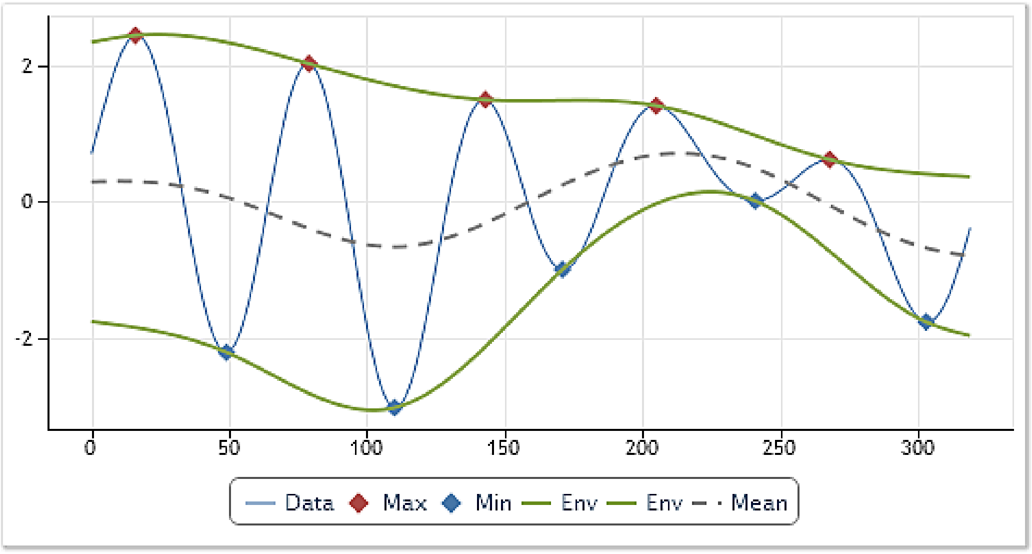

6. if not, repeat step 1-5 with the proto-IMF as the data.
7. if it qualifies as an IMF, assign it as such, and the residue is defined as the data after extracting the IMF.
8. Repeat step 1-7 with this residue as the new data.
9. The operation ends when the residue has no more than one extremum.

Mathematically, this operation can be described as:

$$\begin{gathered}
x(t) - m_{1,1}(t) = h_{1,1}(t); \\
h_{1,1}(t) - m_{1,2}(t) = h_{1,2}(t); \\
\ldots \\
\ldots \\
h_{1,k-1}(t) - m_{1,k}(t) = h_{1,k}(t); \\
\Rightarrow h_{1,k}(t) = c_1(t).
\end{gathered} \tag{2.43}$$

where x is the data, m is the mean of the data, h is the the proto-IMF, and c is the IMF. From equation 2.43, we see that

$$\begin{gathered} x(t) - m_{1,1}(t) = h_{1,1}(t); \\ h_{1,2}(t) = h_{1,1}(t) - m_{1,2}(t) = x(t) - (m_{1,1} + m_{1,2}); \\ \cdots \\ \cdots \\ h_{1,k}(t) = h_{1,k-1}(t) - m_{1,k}(t) = x(t) - (m_{1,1} + m_{1,2} + \ldots + m_{1,k}); \\ \Rightarrow c_1(t) = x(t) - (m_{1,1} + m_{1,2} + \ldots + m_{1,k}). \end{gathered} \tag{2.44}$$

Equation 2.44 show how to extract the first IMF component, and subsequently we have that

$$\begin{gathered} x(t) - c_1(t) = r_1(t); \\ r_1(t) - c_2(t) = r_2(t); \\ \cdots \\ \cdots \\ r_{n-1}(t) - c_n(t) = r_n(t); \\ \Rightarrow x(t) - \sum_{j-1}^{n} c_j(t) = r_n(t). \end{gathered} \tag{2.45}$$

where r is the residue after extracting the IMF from the data. The first residue can be expressed as

$$r_1(t) = \sum_{j-1}^{k_1} m_{1,j} \tag{2.46}$$

and from equation 2.45, we get the expression for our second IMF as

$$c_2(t) = r_1 - r_2 = \sum_{j-1}^{k_1} m_{1,j} - \sum_{j-1}^{k_2} m_{2,j} \tag{2.47}$$

which generalized becomes

$$c_i(t) = r_{i-1} - r_i = \sum_{j-1}^{k_1} m_{i-1,j} - \sum_{j-1}^{k_2} m_{i,j} \tag{2.48}$$

Thus, we see that except from the first one, all IMFs can be expressed as a sum of spline functions, and a basis for the signal can now be expressed in terms of IMFs as

$$\begin{aligned}
x(t) &= \sum_{j-1}^{n} c_j + r_n \\
&= x(t) - \sum_{j-1}^{k_1} m_{1,j} + (\sum_{j-1}^{k_1} m_{1,j} - \sum_{j-1}^{k_2} m_{2,j}) \\
&+ \ldots + (\sum_{j-1}^{k_{n-1}} m_{n-1,j} - \sum_{j-1}^{k_n} m_{n,j}) + \sum_{j-1}^{k_n} m_{n,j} \\
&= x(t).
\end{aligned} \tag{2.49}$$

and equation 2.49 shows us that the original signal is fully and precisely constituted by the IMFs. Since the first IMFs will have the most zero-crossings, it is intuitive that these also are the ones with the highest frequencies. Therefore, IMFs not decompose the signal into separate oscillatory IMF modes, but does it in a way that presents the information in the signal from the highest to the lowest frequencies (much like the detail coefficients in the Wavelet Transform) as seen in Figure 2.10.

One weakness of the EMD, however, is its lack of mathematical rigidity, as it has no analytical solution. For example, one popular choice for the stoppage criterion of the sifting process is the Cauchy type criterion [23], in which the sifting process stops when the difference SD given as

$$SD = \sum_{t=0}^{T} \frac{[h_{k-1}(t) - h_k(t)]^2}{h_{k-1}^2(t)} \tag{2.50}$$

is smaller than some preset small value ε. This can be empirically shown to always hold true when the number of iterations exceeds a certain large value, but it can not be strictly proven mathematically. Another major weakness of the EMD algorithm, is also the phenomena known as mode-mixing. As the name implies, modes with the same frequency content or time scale can be assigned to different IMFs, e.g. when a large amplitude signal contains intermittency with high frequencies [10]. Thus, IMFs with mode-mixing may not always correctly reflect the signal components at different time scales and frequencies, and care should be taken when considering an IMF with respect the possibility of mode-mixing. This is incidentally also the part of EMD where research has focused the most on finding a solution, and interested readers are recommended to read the works of, amongst others, Deering & Kaizer [8], Torres et al. [33] and Wu et al. [39].

Figure 2.10: An EMD done on a noisy signal with significant sine behaviour. The first IMF captures almost all of the high-frequency noise, while IMF2 and IMF3 clearly shows the lower frequency sine components. [19]

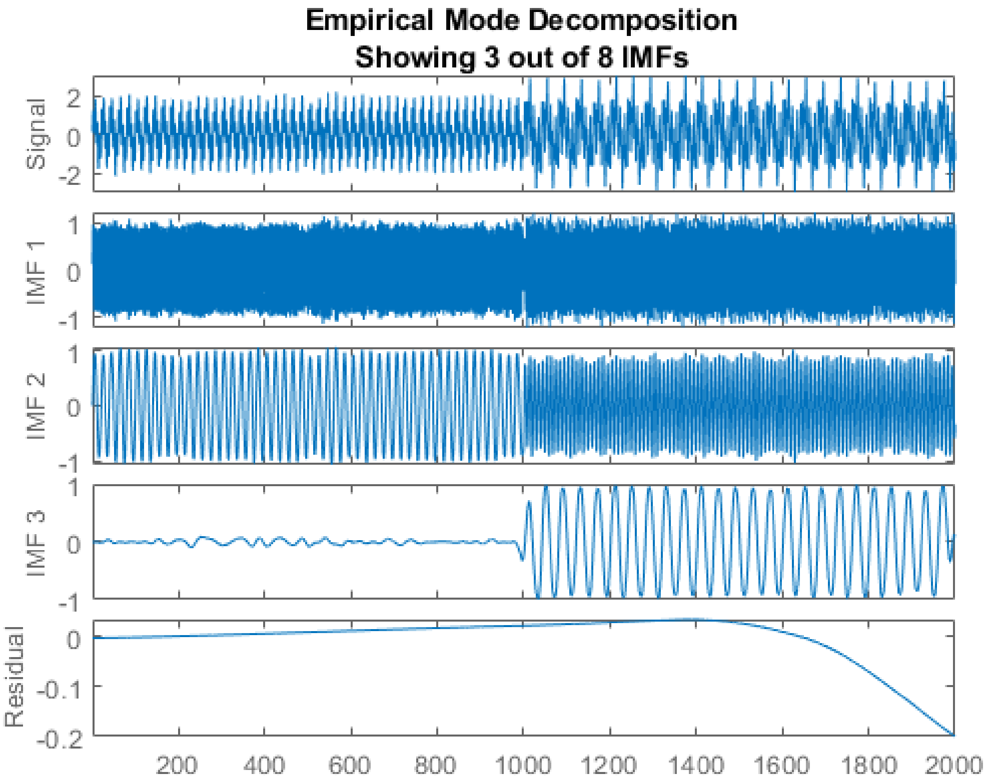

Chapter 3

Methods

The measurements used in this thesis was taken with instruments by ADinstruments. The equipment consisted of an biological amplifier Bio Amp FE132, a three-pack of Shielded Lead Wires MLA2503, and a 3 Lead Shielded Bio Amp Cable MLA2340. The software used for measuring was LabChart 8 for windows, and the programming language used was MATLAB R2017b. The NLMS-filter was implemented using the MATLAB Digital Signal Processing(DSP) toolbox. A dsp.LMSfilter object was created with a filter length of 200, method 'normalized', and a step size 0.001. As a reference signal input to the NLMS-filter, a dsp.FIRfilter object was created with a window based FIR-filter design, implemented using the inbuilt `fir1` function with a filter order of 200, and a lowpass frequency constraint of 0.08 (cutoff frequency 40Hz divided by Nyquist frequency 500Hz). The baseline wandering of the signal was estimated with three different methods. Firstly, a third order Savitzky-Golay filter, using the Matlab `sgol` function with a window length of 2501 samples. Secondly, a maximum overlap discrete wavelet transform using a symlet 4 wavelet and the Matlab `modwt` function with 12 levels of decomposition (in order to capture frequencies as low as 0.1 Hz), followed by a maximum overlap discrete transform multiresolution analysis using the Matlab `modwtmra` function, and summing the last 4 levels. Thirdly, an empirical mode decomposition using the last 4 of the resulting intrinsic mode functions plus the residue as baseline estimate. The algorithm for detecting the QRS-complexes was implemented using first, as for the baseline estimation, a `modwt` and `modwtmra` approach using a symlet 4 wavelet down to the 10th level[1]. The magnitude and location of the peaks was then found by using the 5th level of the resulting transforms as input to the Matlab `findpeaks` function, with 'minpeakprominence' of the peaks set to 0.0001, and 'min-

---

[1] though this choice was arbitrary, as any level of 5 or below would have sufficed

peakdistance' between peaks set to 200. the separation of the ECG-signal into heart cycles was done by using the R-peak location as the base, and then cutting off the signal at each side of this point at a distance equal to half the mean heart rate (e.g. with sampling frequency 1000Hz, and mean heart rate 80 BPM, the cutoff distance would be ((60/80)*1000)/2 = 375). As the first part of artifact classification, a threshold of 1.5 was used, where if any R-peak location occurred later than 2*cutoffDistance*threshold, a cycles worth of signal would be extracted at the midpoint between the last and current R-point locations and treated as an artifact. In the second part of the artifact classification, an initial reference cycle was created by taking the mean of the 20 first separated cycles. For each new consecutive cycle occurring, a normalized cross-correlation was done between this cycle and the reference cycle using the Matlab `xcorr` function with normalization option 'coeff'. A threshold value of 0.97 was chosen, and if the max value in the cross-correlation sequence matched or exceeded this value, the current cycle would be classified as normal, and a new updated reference cycle would be created using the current cycle together with the preexisting ones. If the threshold was not met, the cycle would be classified as an artifact and put in a separate matrix together with the artifacts classified in the cycle separation. Lastly, in the part concerning EDR estimation, the HRV was extrapolated over the measurement duration using the R-peak locations as input data, and compared to the filtered ECG-signal. A power spectrum was also made of the HRV signal in order to analyze its frequency content.

Chapter 4

Results and Discussion

4.1 NLMS-filtering

The Filter showed an overall high performance in reducing the noise values for the different subjects, and Figure 4.1-4.2 shows a 10-second extract of both the raw signal and the filtered signal, while Figure4.8 shows the fast fourier transform power spectrum after filtering. The results for Subject 1 (Fig:4.1) are enlarged in order to show a more detailed example of the filter performance. Not surprisingly, the measurements that were of "better" quality, yielded better results then passed through the filter, as seen in, for example, Figure 4.1 and Figure 4.3, where the noise is predominantly power line interference. Even in the measurements that showed more stochastic behavior such as Figure 4.5a and Figure 4.2a, the filter performance significantly removes the high-frequency noise. However, for subject 4, the measurements were done under less than optimal conditions, where recent strenuous activity caused extensive respiratory movement and muscle noise, and moist skin due to sweat made for difficulties in electrode placement. The result is seen in Figure 4.4a, where one can see large amounts of stochastic noise in the signal, and the corresponding filtered signal in Figure 4.4b shows that the NLMS-filter, though performing admirably, struggles in locating the optimal solution when the stochastic nature of the environment it is operating in surpasses a certain threshold. On the positive side, the post-filtered signals does not seem to change their shape in any significant way[1], and the different waveforms and complexes are shown clearly with minute amounts of noise, which is important both for the methods in this thesis, and also for future

---

[1] However, there exists the possibility of information being distorted even from these small changes, so depending on how strict one wishes to be with respect to conserving information, it might be worth considering an alternative method for high-frequency removal.

implementations. Note that some degree of ringing still occurs, most noticeably seen in Figure 4.1b in the onset of each QRS-complex. This is due to the Gibbs phenomenon, and will most likely be impossible to fully remove in any filter operation that employs an IIR-filter. Also, as seen from the power spectra in Figure 4.8, some subjects show frequency content slightly above the cutoff frequency of 40 Hz, and a slightly lower cutoff frequency might be considered if one is able to safely avoid encroaching on the QRS-complex frequency domain.

Figure 4.1: Filter results for subject 1. Note that the ventricular heartbeat does not affect the filter performance noticeably

(a) Raw signal subject 1

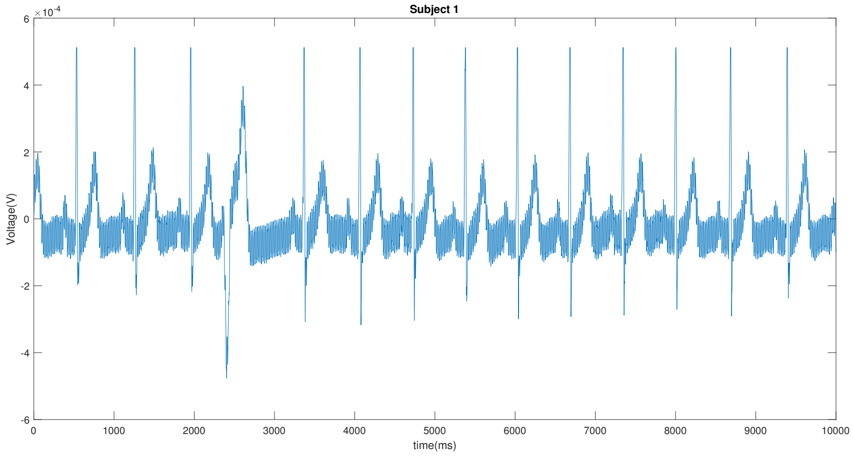

(b) NLMS filtered signal subject 1

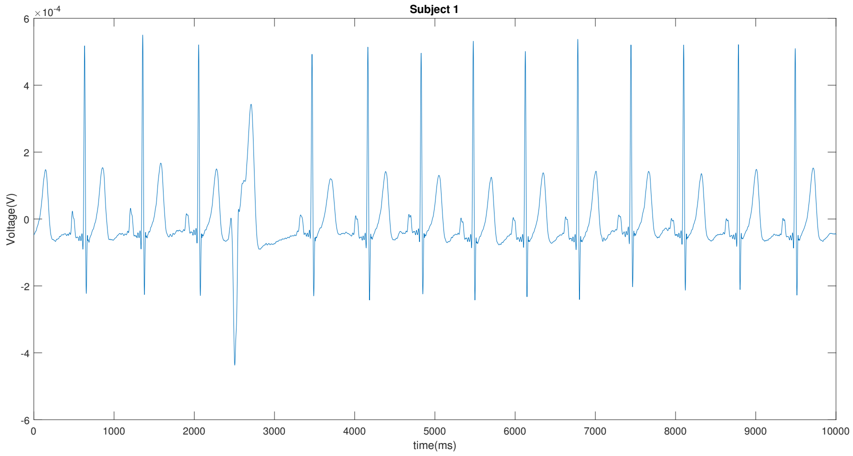

Figure 4.2: Filter results for subject 2

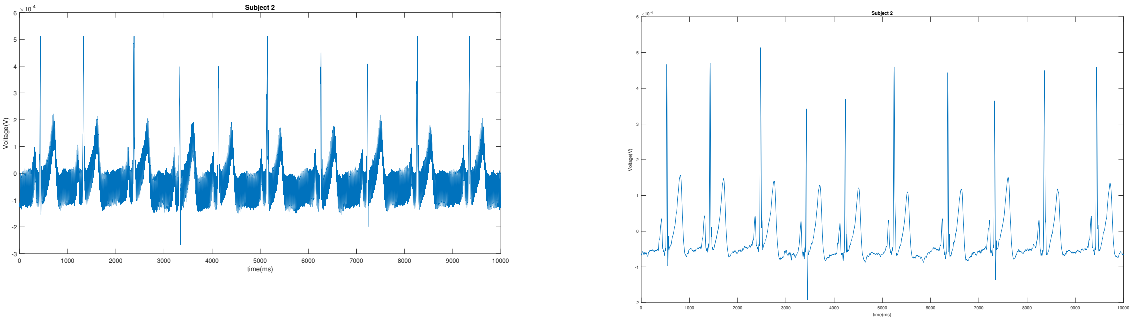

(a) Raw signal subject 2

(b) NLMS filtered signal subject 2

Figure 4.3: Filter results for subject 3

(a) Raw signal subject 3

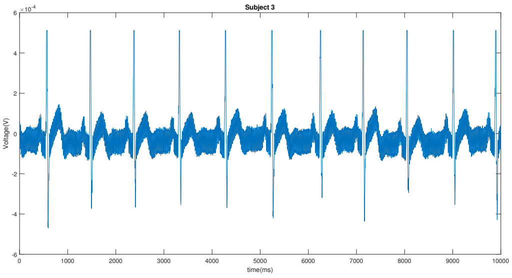

(b) NLMS filtered signal subject 3

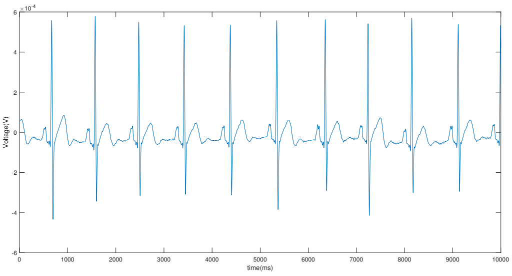

Figure 4.4: Filter results for subject 4

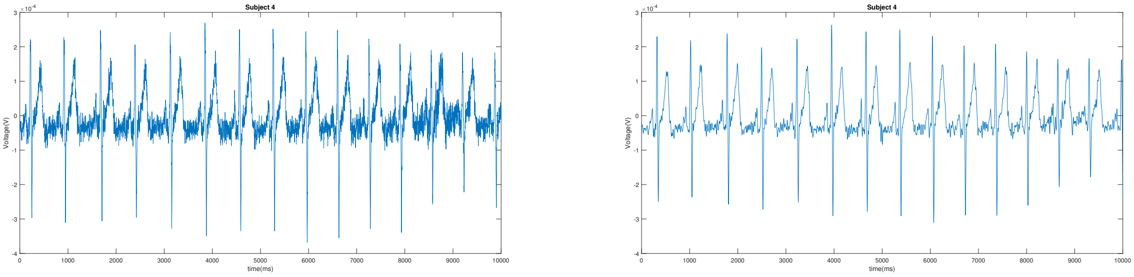

(a) Raw signal subject 4

(b) NLMS filtered signal subject 4

Figure 4.5: Filter results for subject 5

(a) Raw signal subject 5

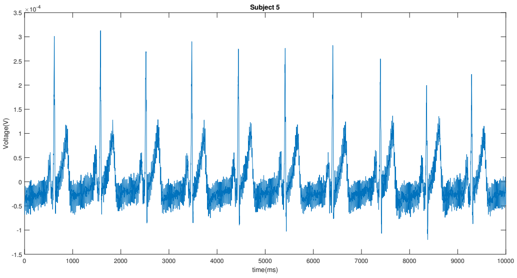

(b) NLMS filtered signal subject 5

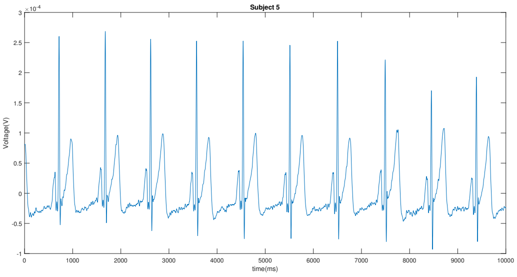

Figure 4.6: Filter results for subject 6

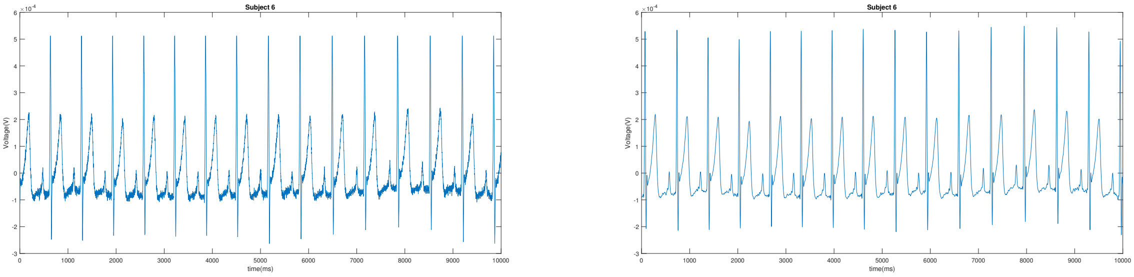

(a) Raw signal subject 5

(b) NLMS filtered signal subject 6

Figure 4.7: Filter results for subject 7

(a) Raw signal subject 7

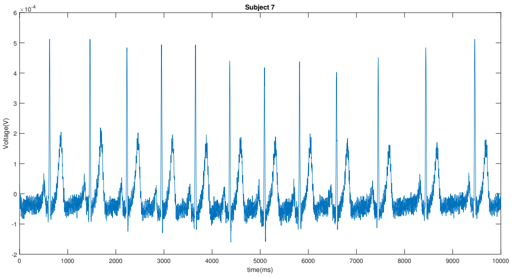

(b) NLMS filtered signal subject 7

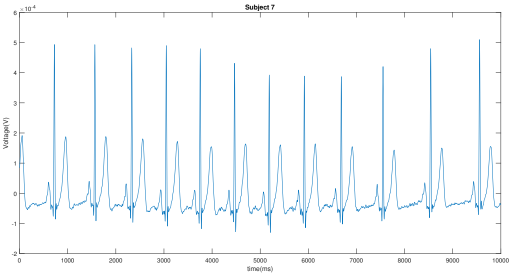

Figure 4.8: FFT power spectrum for the different subjects

(a) Subject 1 (b) Subject 2

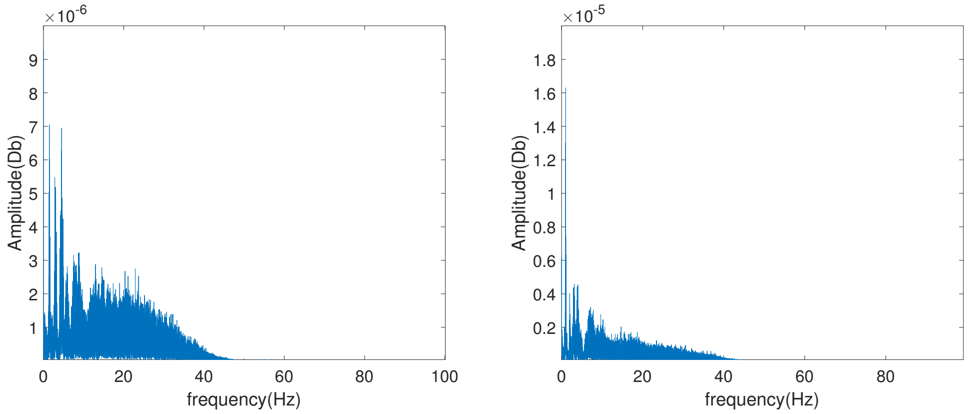

(c) Subject 3 (d) Subject 4

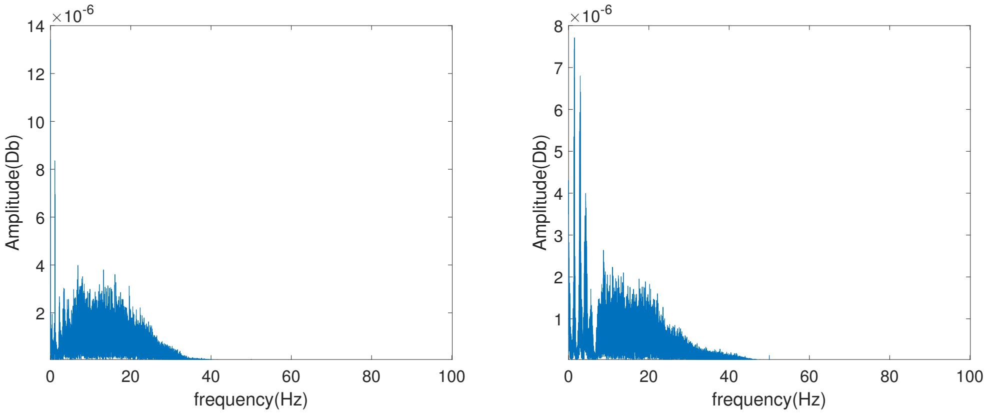

(e) Subject 5 (f) Subject 6

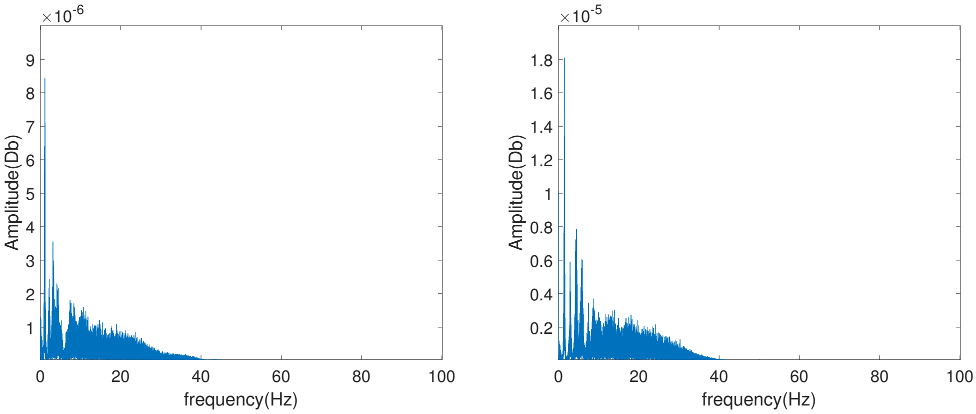

(g) Subject 7

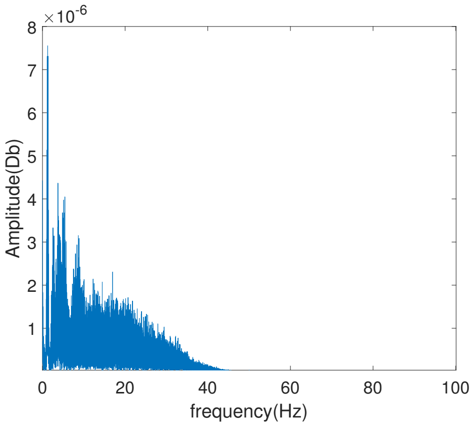

4.2 Baseline wandering identification and removal

Though using quite different methods, both Savitzky-Golay, DWT, and EMD performed fairly well in estimating the baseline wandering and shifts of the different subjects, as seen in Figures 4.9-4.15. The figures show the first 100 seconds of the post NLMS-filtered ECG-signal with the estimated baseline plotted on top, and as both the R-peaks and T-peaks have some inherent variability in them, the baseline wandering is most clearly seen from the changes in the P-wave (the shortest of the peaks among the peaks in the signal). While some subjects had little baseline wandering to begin with, such as Subject 14.9 and Subject 44.12, others such as Subject 24.10, Subject 34.11 and Subject 54.13 showed a much larger degree of fluctuation, and performance-wise, the EMD estimated baseline performs less accurately in baseline estimation compared to the two other methods, especially on catching baseline shifts as seen in Figure 4.13. However, this is most likely due to mode-mixing or improper choice of which intrinsic mode functions to extract, and with more refinement, EMD would quite probably yield as good a result as for the other methods. Regarding Savitzky-Golay and DWT, they show similar behavior, with DWT on the overall performing markedly better, as especially seen in Figure4.9 and Figure4.14, with the noticeable exception of Figure4.15, where Savitzky-Golay outperforms DWT slightly. As seen from Subject 2 in Figure 4.10, The Savitzky-Golay estimated baseline shows for some subjects a slightly oscillatory behavior, due to the third degree of its filter order. This is unwanted, as it can affect the morphology of the signal when extracted, but lower order filter performs more poorly with respect to following baseline shifts, making it a trade-off in terms of baseline accuracy versus signal distortion. More tuning of the filter by varying window lengths is also a possibility, but for the rest of the thesis, the baseline will be extracted using the DWT method. Also note how the DWT estimated baseline centers itself around zero, while the Savitzky-Golay and EMD estimated baseline more closely overlaps with the signal, as most clearly seen in Figure4.10 and Figure4.15. This is due to

Figure 4.9: Baseline estimates for subject 1

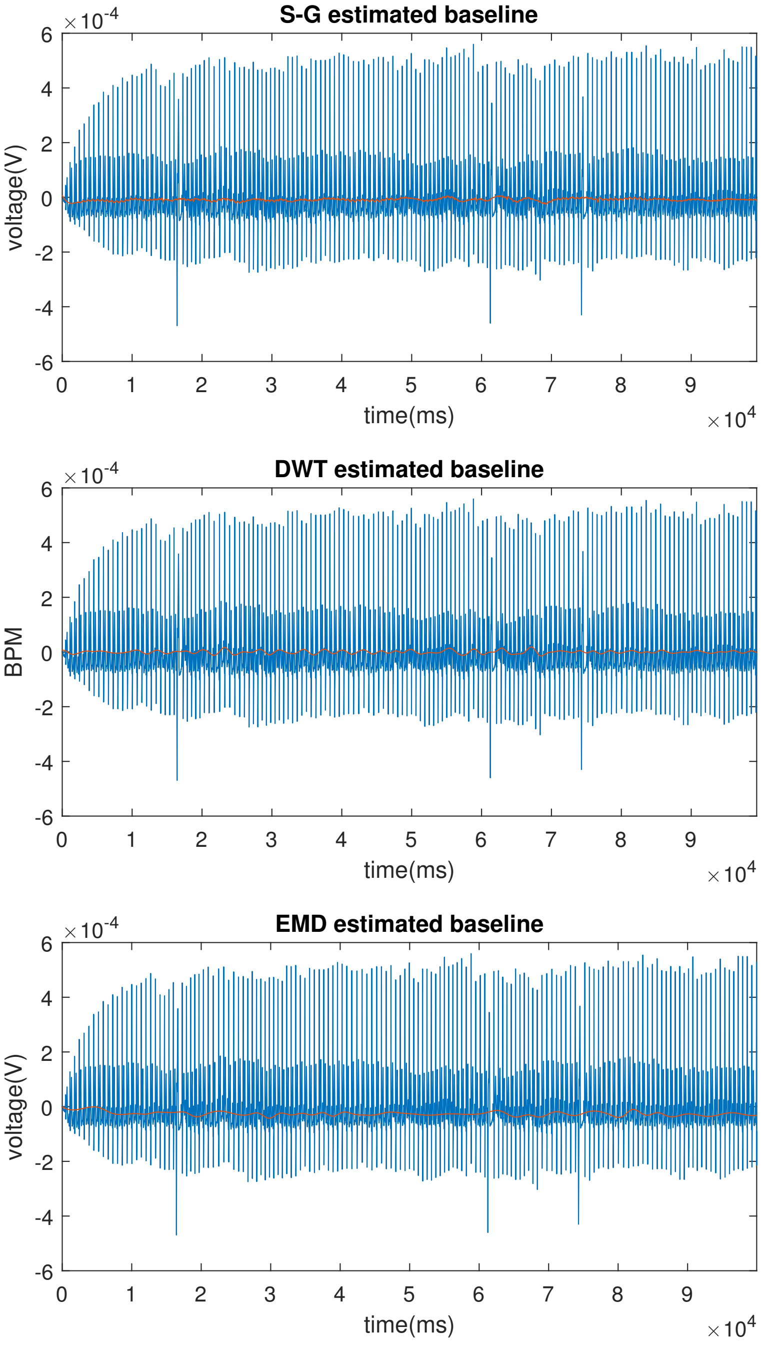

Figure 4.10: Baseline estimates for subject 2

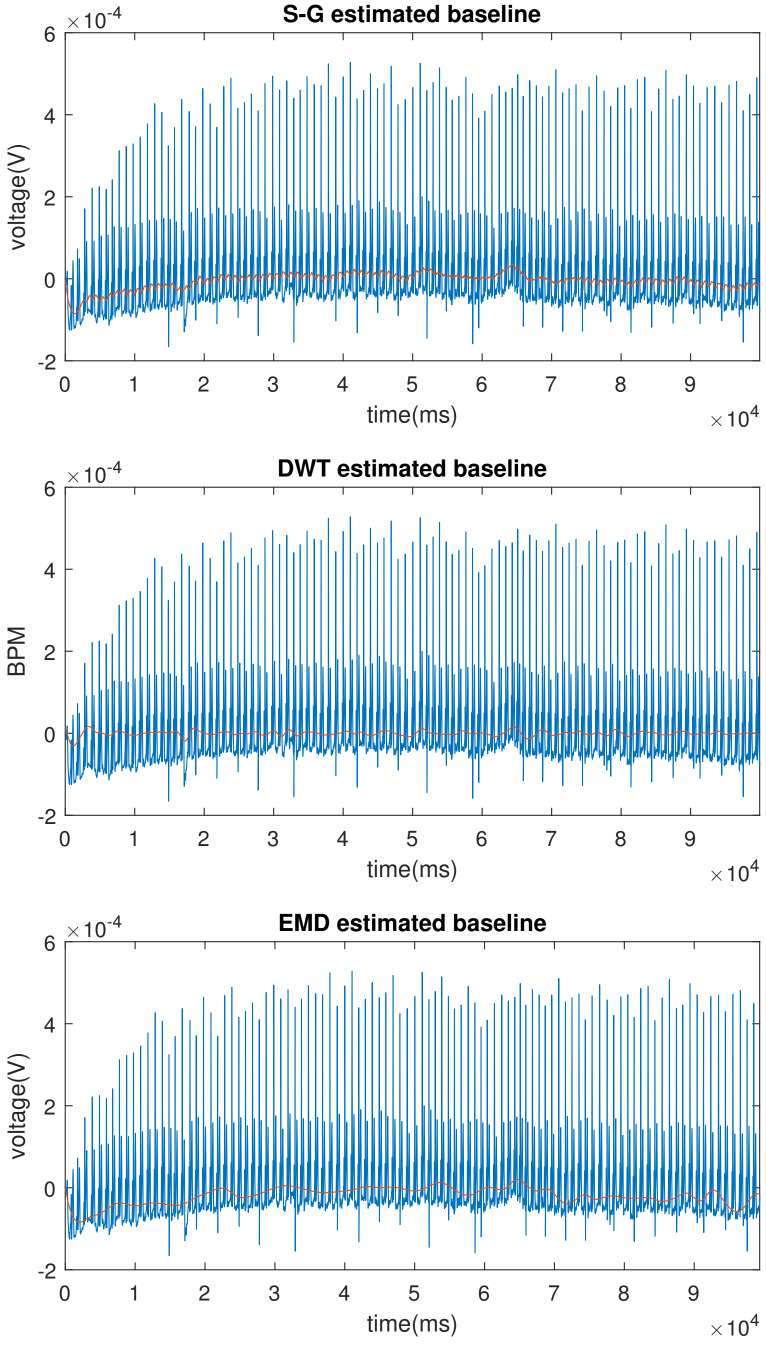

Figure 4.11: Baseline estimates for subject 3

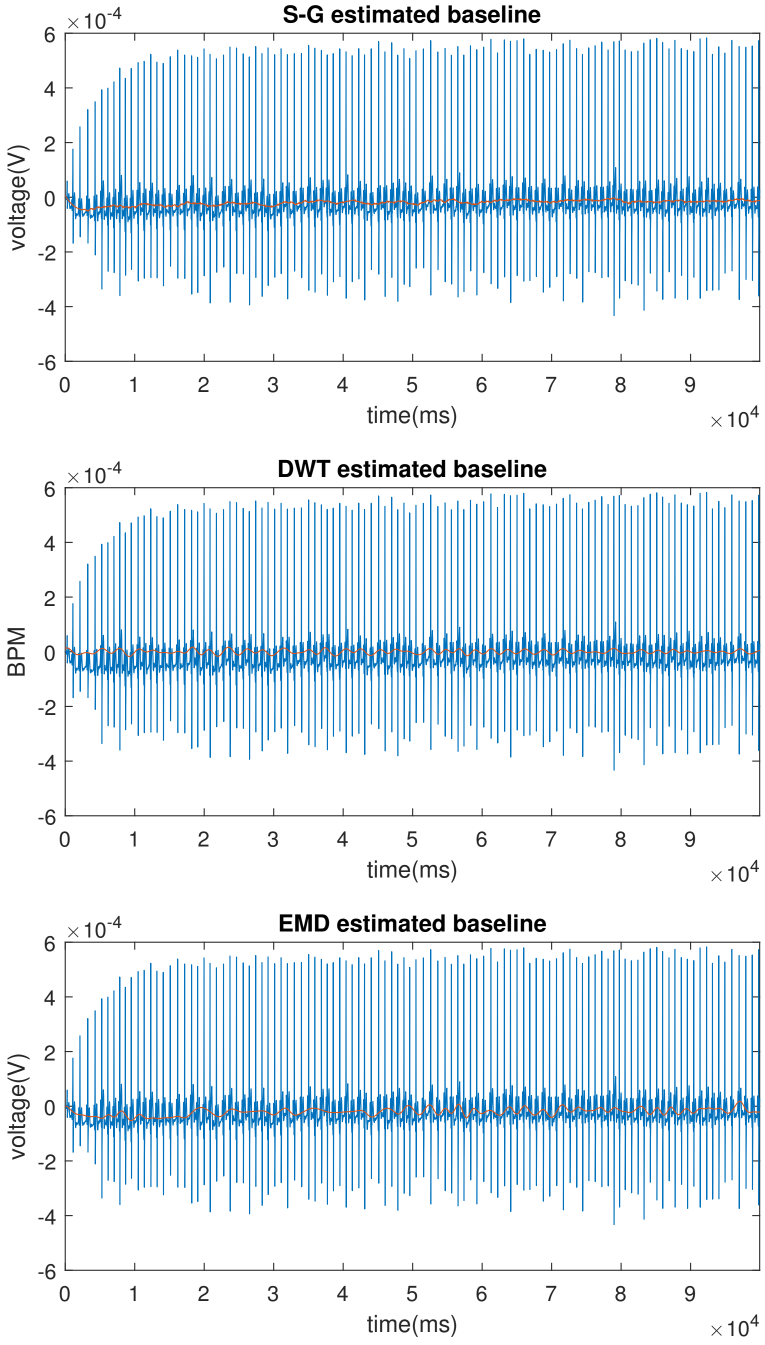

Figure 4.12: Baseline estimates for subject 4

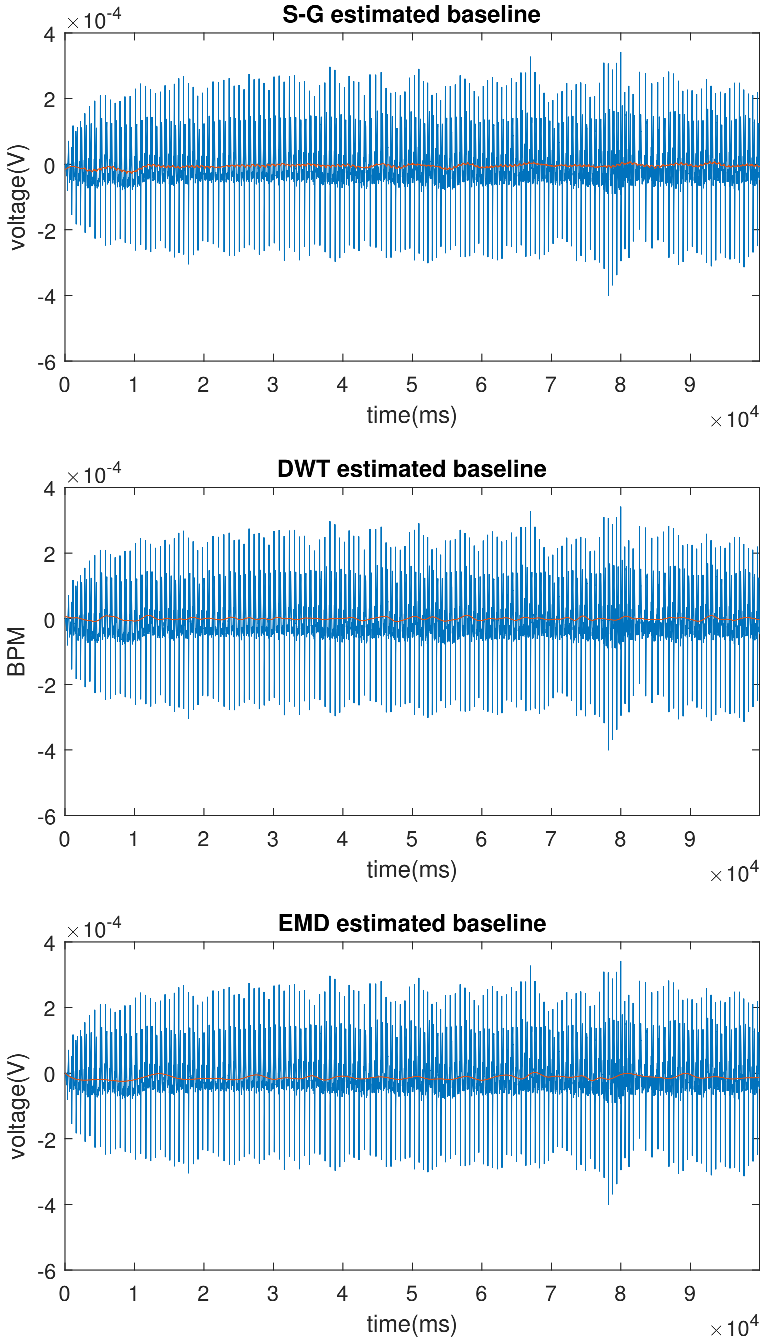

Figure 4.13: Baseline estimates for subject 5

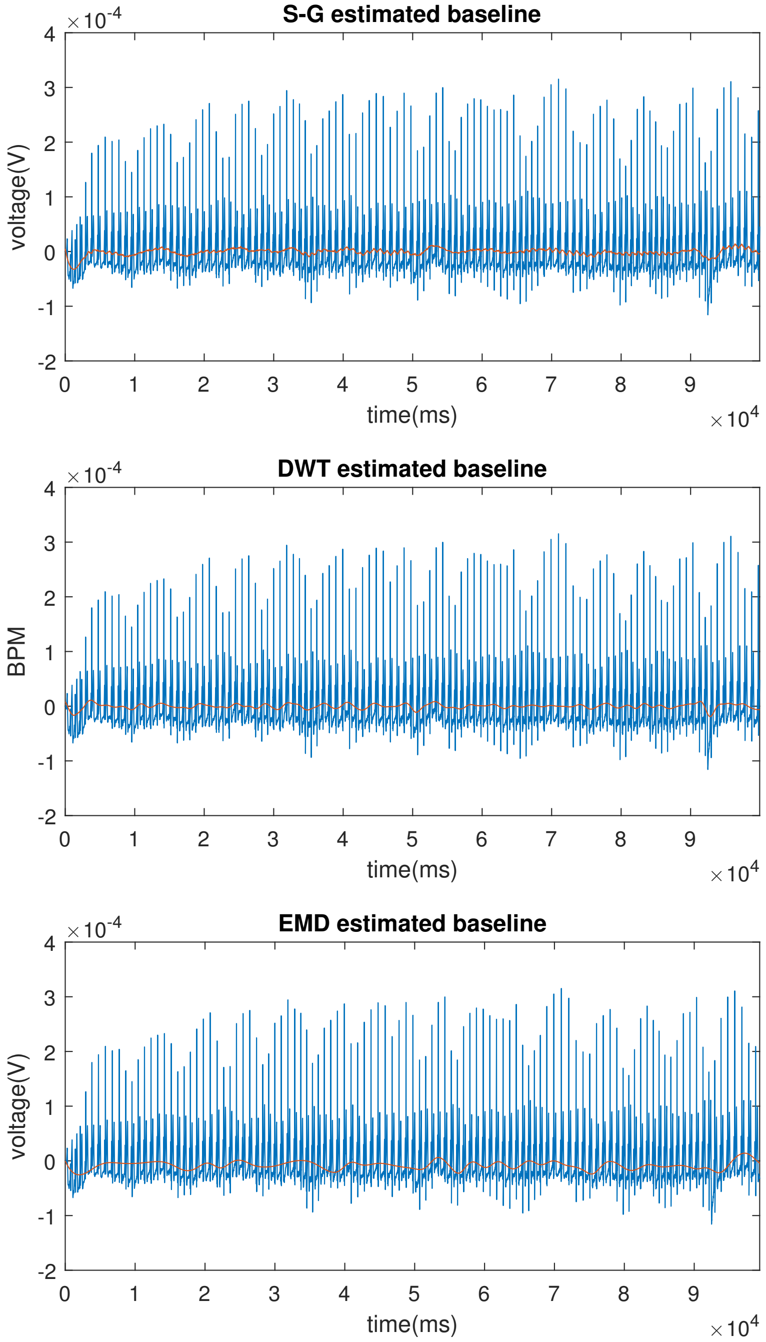

Figure 4.14: Baseline estimates for subject 6

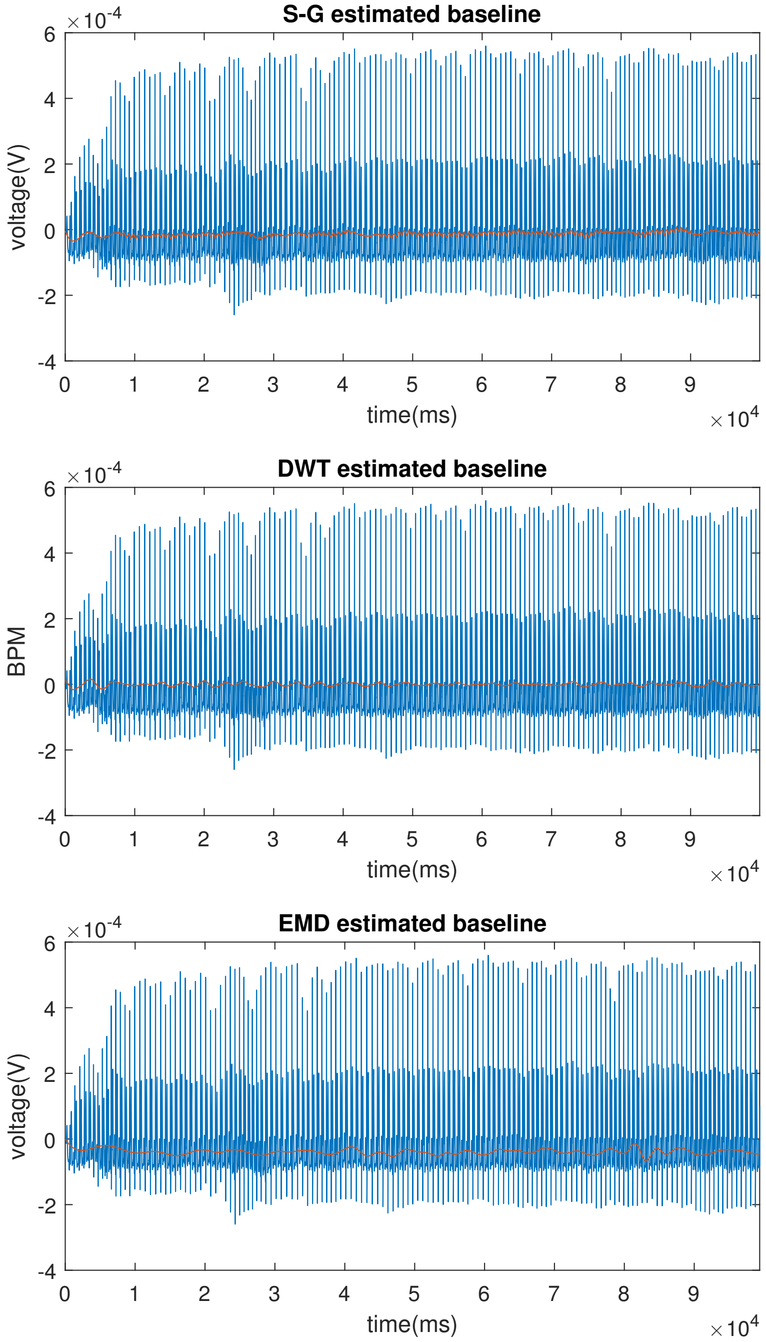

Figure 4.15: Baseline estimates for subject 7

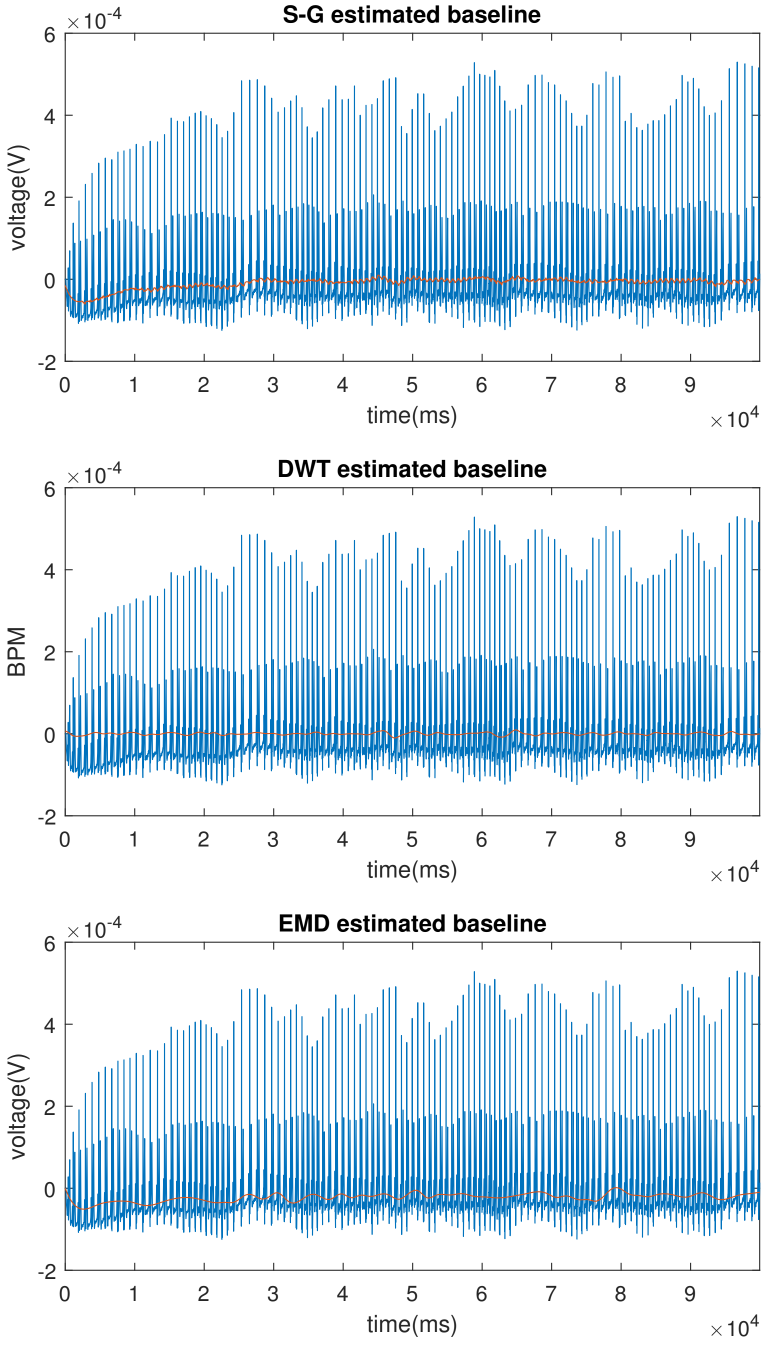

4.3 QRS-complex detection

The goal of the QRS-complex detection was met with a large degree of success, and the use of DWT with a sym4 wavelet proved to be a highly efficient method for detecting the different heartbeats. In Figure 4.16, the fifth level wavelet transform is plotted on top of the ECG-signal, showing how each R-peak results in a sharp increase in the transform value due to the high correlation between the QRS-complex and the sym4 wavelet, and the position of this peak transform value is then marked on the ECG-signal with a red circle, showing a high degree of accuracy in peak-detection. The ventricular heartbeat in the middle has little correlation with the wavelet, as seen from its transform value, and it is therefore correctly not marked as a QRS-complex. The 10-minute NLMS-filtered and baseline adjusted signal for each of the seven subjects is shown in Figure 4.17a-4.17g, and the detected QRS-complexes are marked as red circles. Some subjects, and especially Subject 1 (Fig:4.17a) and Subject 3 (Fig:4.17c), shows very little variation in the R-peak values, and with distinct differences between the R-peaks and the P- and T-wave, a comparably good result could probably have been achieved by simply using the built-in `findPeak` function in Matlab. Since the DWT does not consider baseline offset in its calculations, however, the implemented method performs remarkably well in the signals with large differences between R-values, such as Subject 5,6 and 7 (Fig:4.17e-4.17g). In addition, it achieves equally good results on Subject 4 despite the much larger noise content remaining in the signal, indicating that the method is quite robust as well, as long as the distinct QRS-complex shape is not noticeably distorted. Note also that the beginning of every signal has significantly lower peak values compared to the rest of the signal. This is due to the NLMS-filter needing some amount of time (approx. 4-5 beats) in order for the error to converge to zero, and while the QRS detection method performs admirably in catching even these early heartbeats, they are actually unwanted in the sense that they are too artificially altered (by the filter) to represent the accurate shape of the heartbeat. Though they will be promptly removed by later stages of the pre-processing, it might, therefore, be better to start the QRS-detection algorithm first after the NLMS-filter has converged.

Figure 4.16: ECG-signal extract from subject 1, showing the wavelet transform value at different parts of the signal. The ventricular heartbeat in the middle does not have a typical QRS-complex form, and therefore yields a low transform value.

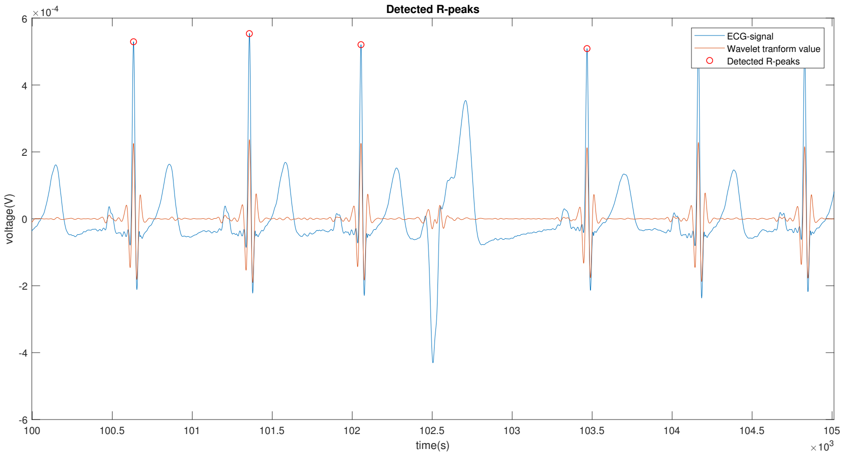

Figure 4.17: QRS-detection results

(a) QRS Subject 1

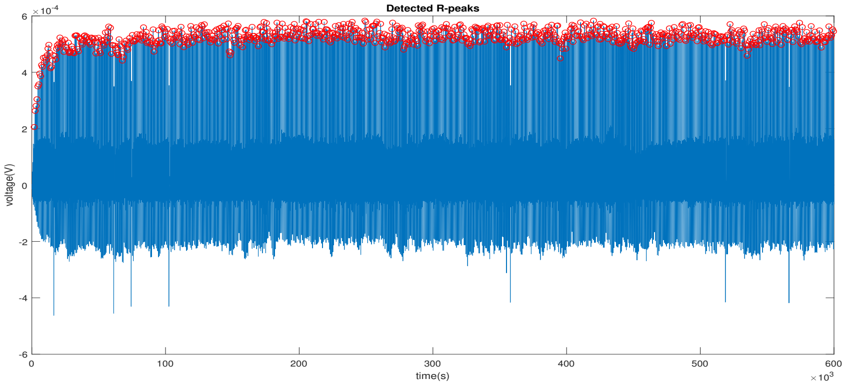

(b) QRS Subject 2

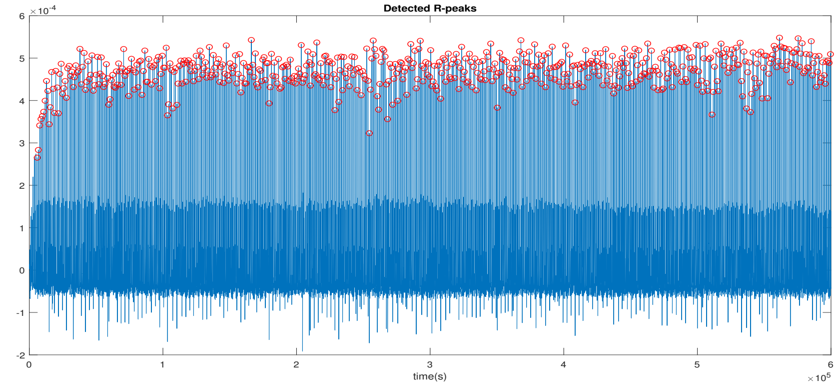

(c) QRS Subject 3

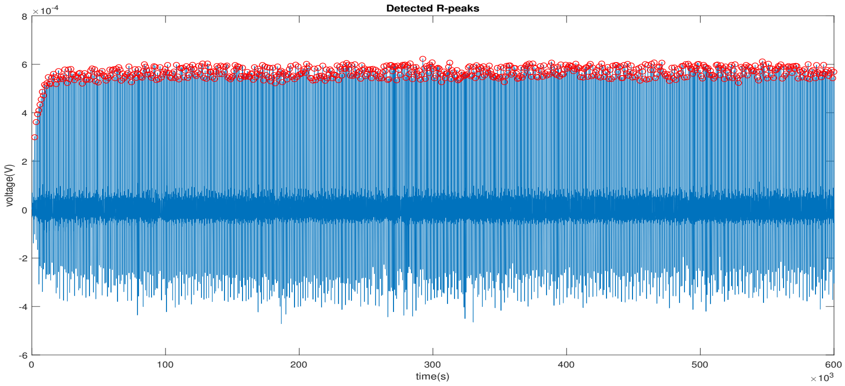

(d) QRS Subject 4

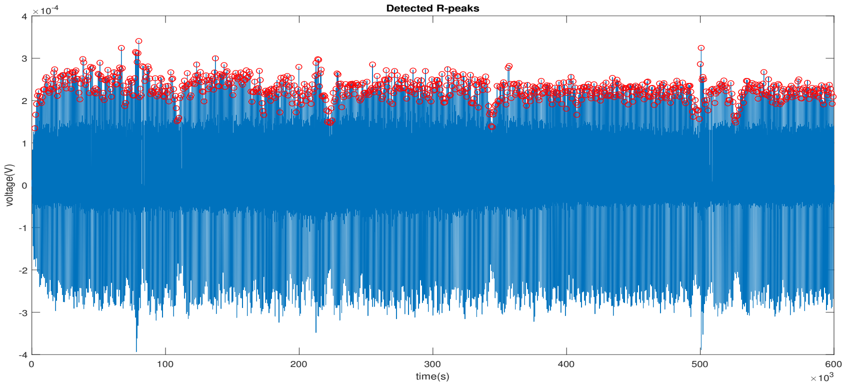

(e) QRS Subject 5

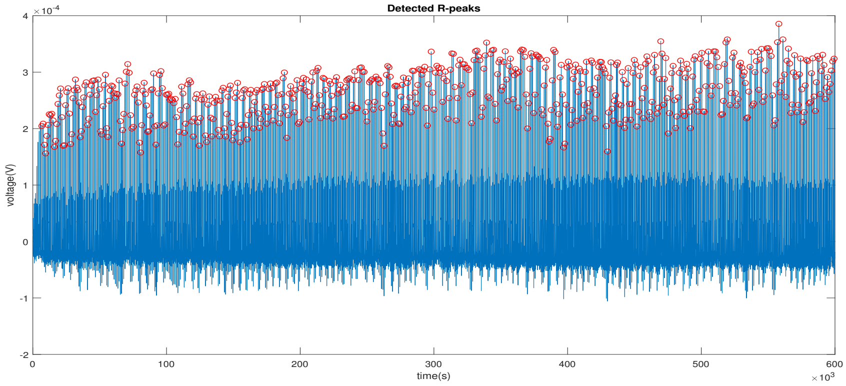

(f) QRS Subject 6

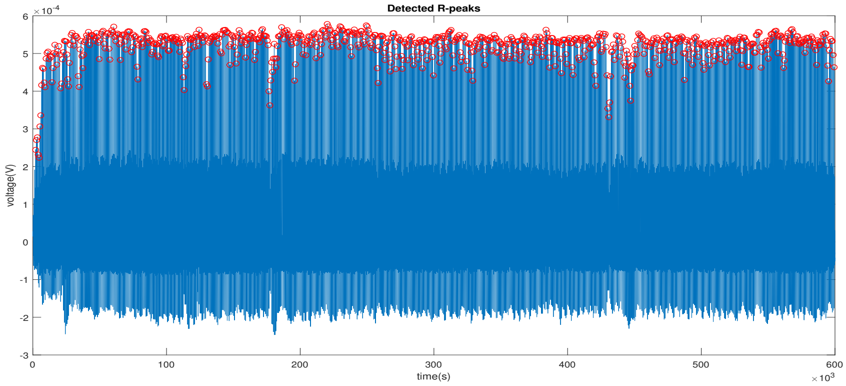

(g) QRS Subject 7

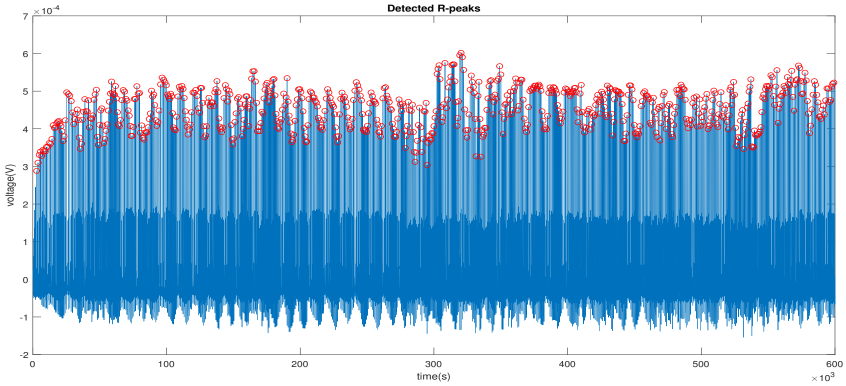

4.4 Separation of the ECG-signal into separate heartbeats

The results of separating the signal into samples based on the separate heart beat cycles are shown in Figure 4.18-4.24, where columns of three show respectively the samples deemed to be artifacts, the "normal" samples, and the initial and final reference sample used in determining whether or not to label a sample as an artifact. The algorithm for determining artifacts was, as mentioned earlier in the thesis, twofold, and in Figure 4.18, we can see that the first part resulted in all the ventricular heartbeats having been correctly identified as artifacts even though they never were marked as QRS-complexes. The other part of the algorithm, with samples being consecutively cross-correlated against a reference sample, worked arguably well, depending on what one defines as a "normal" sample. For example, in Figure 4.19, a high number of approximately 8.2% of the samples were marked as artifacts, and though some of the samples noticeably deviate from the other samples, most still have the characteristic form one would think would pass for a good sample. There are two chief observations to be made here. Firstly, both the initial and final reference sample clearly indicates an inverted S-wave, in fact, the final reference sample shows that the more samples you use in creating a reference, the more distinct this inversion becomes. Secondly, the overall height and depth of respectively the R-peak and S-wave of the artifacts are lower when compared to the samples. Thus, a sample that might be seemingly normal, will still be classified as an artifact if the amplitude at any of the waves or complexes differ markedly from the amplitudes of the reference. Conversely, a sample that might appear to be odd, as especially seen occurring in the samples in Figure 4.18,4.21 and 4.24, can be classified as a normal sample as long as it deviates only at that temporal location (or very little at several locations), and accurately follows the reference sample the rest of the time. The prime example of this is Subject 4 (Fig:4.21), whose samples seem at first glance rather erratic and turbulent. Interestingly, the reference samples show that the underlying shape of the heartbeat is actually quite defined and distinct, not showing any distortion compared to the other subjects, and an inspection of the initial and final reference sample shows that the small expected fluctuations found in the beginning evens out as the samples are being processed. Though the aforementioned amplitude variance also plays into artifact classification, this shows thus that most of the cycles are well-behaved, with the few erratic only being temporally so. Another observation to be made, and which is a logical extension of earlier observations, is that the subjects with the fewest classified artifacts

(Fig:4.18,Fig:4.20,Fig:4.23 and Fig:4.24) also have the least R-peak variance, as seen in Figure 4.17a,4.17c,4.17f and 4.17g, with the noticeable exception of Subject 7, those small degree of artifact classification is likely due to consistent and well-behaved cycles. All this together might, therefore, indicate that the current implementation of artifact classification is slightly sensitive towards ECG-signals containing high variance in R-peak magnitude, and some adjustment will probably be considered with specific respect to R-peak magnitude. An undesirable trait that showed up can be seen in the samples of Subject 1,4,6 and 7 (Fig:4.184.23), where at the beginning of the samples, some of them have a slight overlap with the previous sample. Observing the heart rates (Fig:4.25a-4.31a) of these subjects yields a rather straightforward explanation, in that both the mean heart rate and the difference between local heart rates are significantly higher than for the other subjects. Thus, by separating samples a set distance defined by the mean heart rate, some samples will slightly overlap if the maximum temporal heart rate differs from the mean heart rate above a certain value, and conversely, some samples will not manage to catch the whole cycle if the minimum temporal heart rate differs from the mean heart rate below a certain value. Interestingly, the P-wave of Subject 6 shows significant shifting back and forth, and since this point is located well away from the ends of the cycles, this is likely behaviour independent from the cycle overlapping. Exactly what causes this shifting can only be theorized for now, but this is exactly the type of phenomena that would be interesting to study further in an multivariate analysis.

Figure 4.18: Artifacts, Samples and References for subject 1

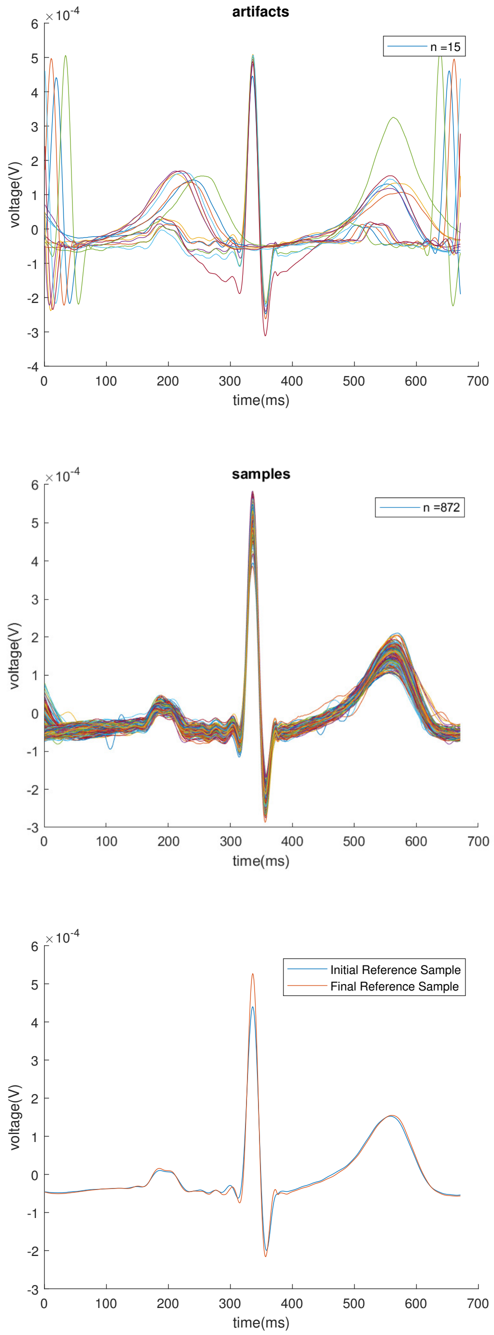

Figure 4.19: Artifacts, Samples and References for subject 2

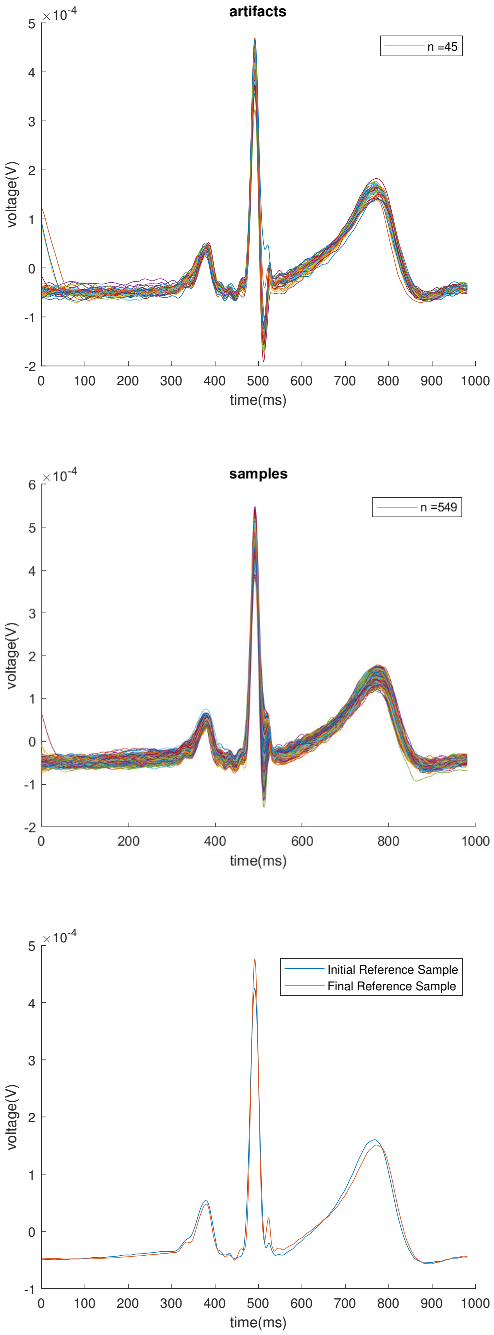

Figure 4.20: Artifacts, Samples and References for subject 3

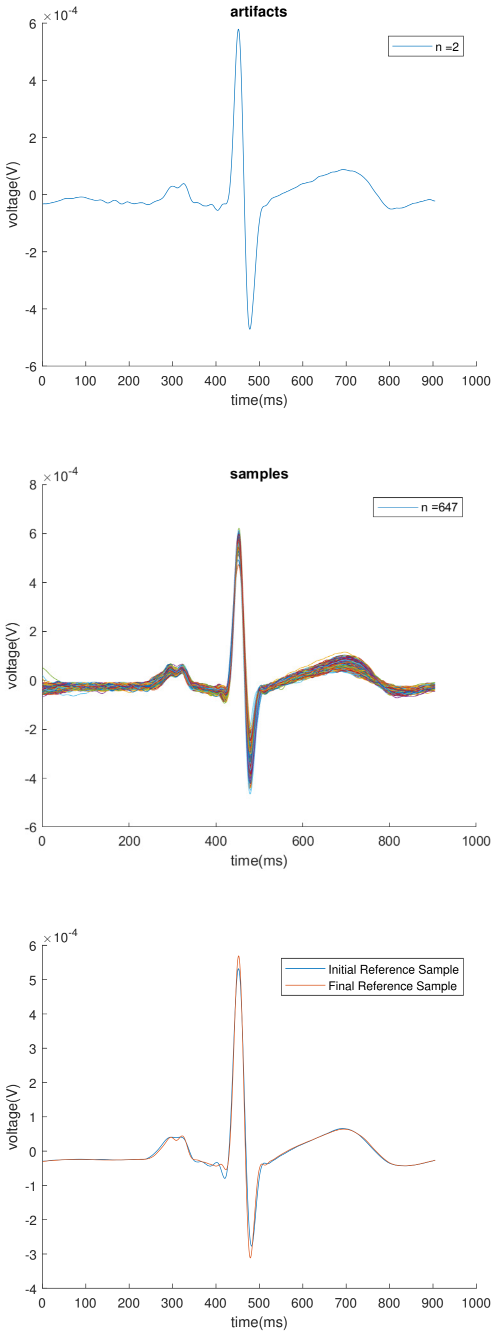

Figure 4.21: Artifacts, Samples and References for subject 4

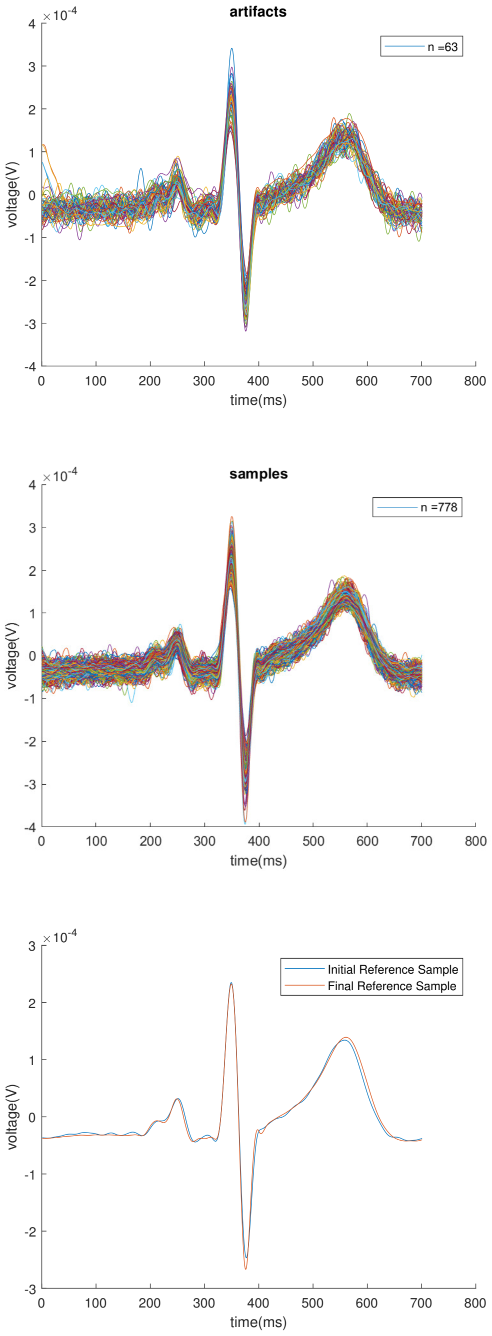

Figure 4.22: Artifacts, Samples and References for subject 5

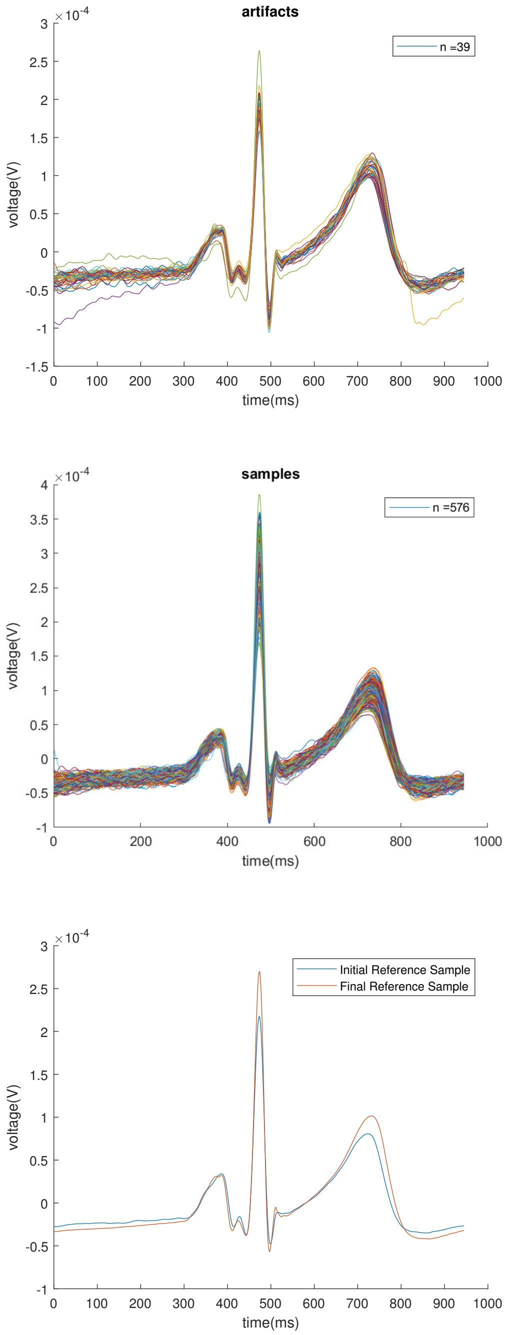

Figure 4.23: Artifacts, Samples and References for subject 6

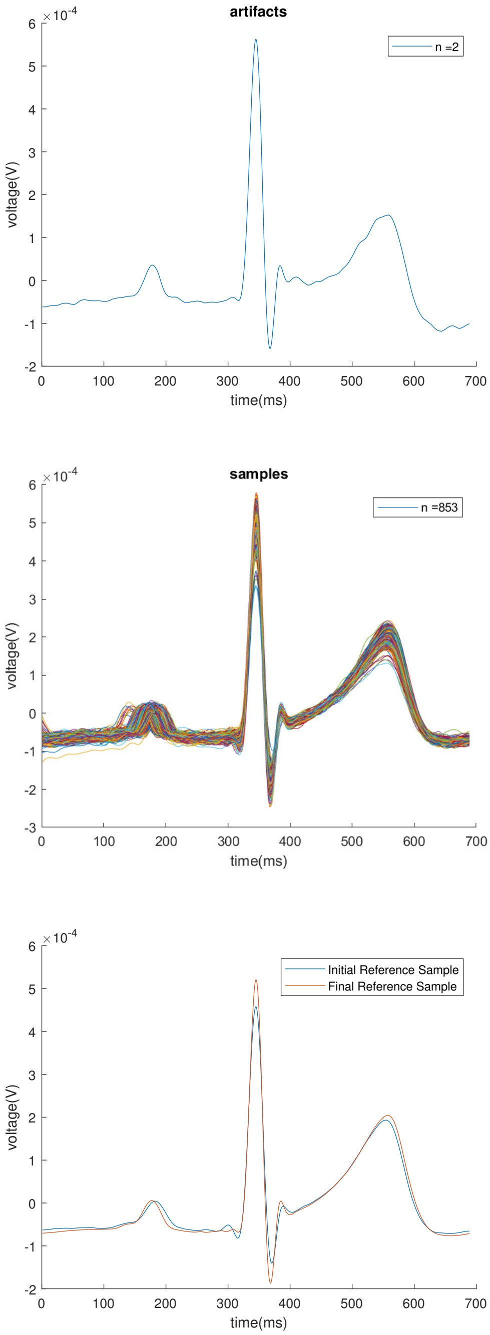

Figure 4.24: Artifacts, Samples and References for subject 7

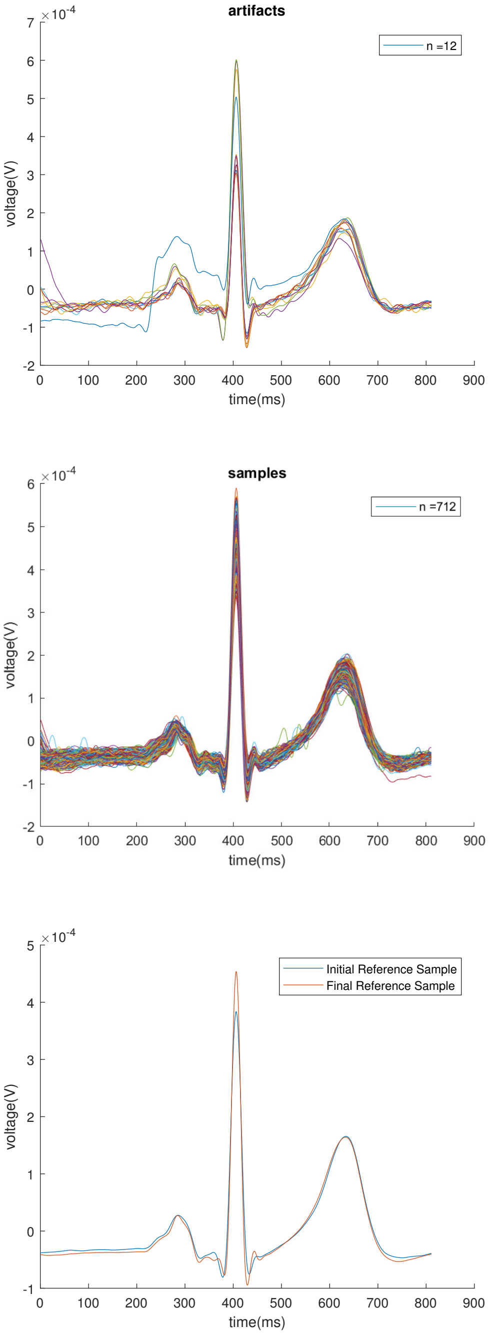

4.5 Determining respiration rate

As mentioned earlier in the thesis, accurately determining the respiration rate was hard without some reference respiratory signal gathered from e.g. a respiratory belt. Empirically, by observing the subjects under the measurements, a ballpark estimate of the respiration was done that placed the respiration rate at about 0.1 Hz to 0.2 Hz. In Figure 4.25-4.31, the heart rate variability found from the detected R-peaks is plotted together with its corresponding Power spectrum, and as immediately seen in Subject 1 (Figure 4.25), the HRV is highly influenced by how consistent R-peaks are detected, with the sudden drops in HRV corresponding to the premature ventricular heartbeats. While it is quite possible to compensate for this (e.g. by manually inserting some mean value whenever an expected R-peak is not detected), the overall result will not change markedly as long as number of non-typical QRS-complexes remains low. In this case, it holds especially true as we are more concerned with the long-term trends (respiration) than local phenomena (ectopic heartbeats). It is, however, most likely a contributor to the high peaks in the very lowest frequencies in Figure 4.25b, and must be remembered when considering the power spectrum. Regarding the different spectra, it is, not surprisingly, hard to spot the EDR as a single frequency or a narrow frequency band. This is due to the differences between the subjects during measurements, with some, such as Subject 3 and 5 (Figure4.27 and Figure4.29) talking and laughing several times during the measurements, and others, especially Subject 6 and 7 (Figure4.30 and Figure4.31) sitting very still while breathing slowly and steady. Observing the power spectrum for Subject 6 and 7 in Figure 4.30b and Figure 4.31b reflects this by showing significant peaks at approximately 0.1 Hz, which closely corresponds to the respiration rate that was observed during measurements. This can also be seen in the corresponding HRV, with steadier clearer sine movement patterns than for the other subjects. Subject 2 and 4 (Figure4.26 and Figure4.28) also shows frequency content around that region, but it is much more distributed, or the peaks are not significant enough to be clearly determined. One interesting observation worth noting, is that except from Subject 5, all the power spectra shows similar patterns. They start with some larger peaks in the lowest frequency range followed by a dip in power, and then comes back more strongly again upon entering the respiration frequency range. The peaks around 0.1 Hz-0.2 Hz were of course expected, but the powerful low frequencies is a bit harder to explain. A theory is that they may be connected to ultra-low-frequency physiological oscillations, but this is as of now only a conjecture.

Figure 4.25: HRV subject 1

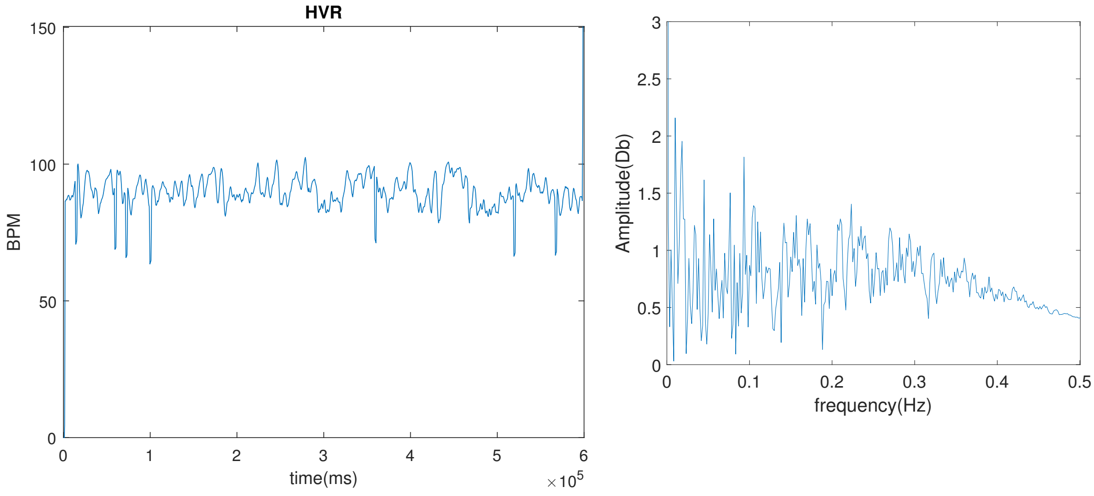

(a) Heart rate

(b) HRV power spectrum

Figure 4.26: HRV subject 2

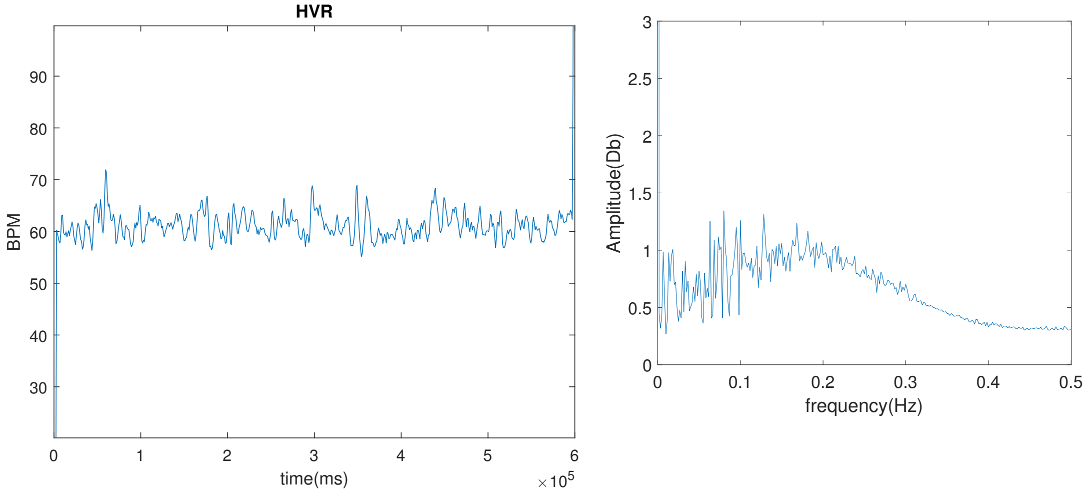

(a) Heart rate

(b) HRV power spectrum

Figure 4.27: HRV subject 3

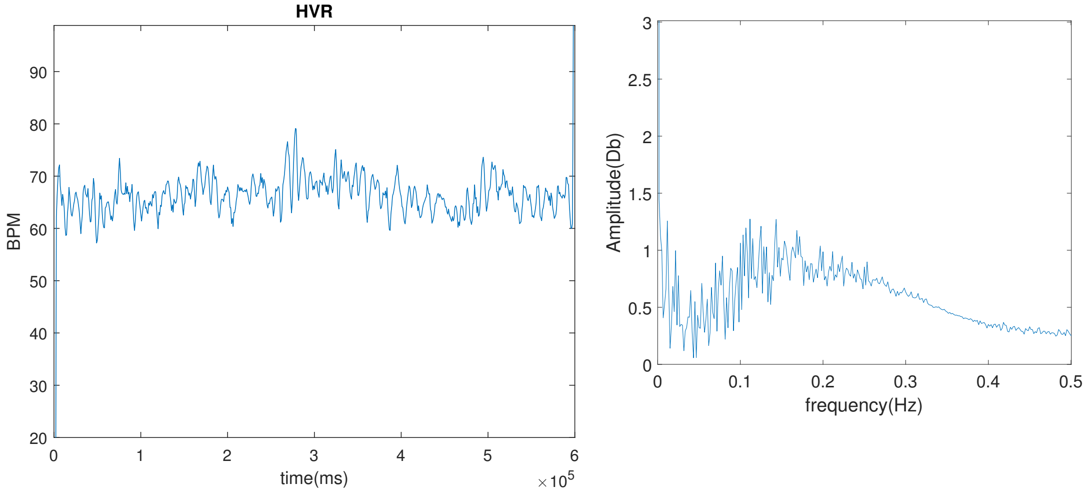

(a) Heart rate

(b) HRV power spectrum

Figure 4.28: HRV subject 4

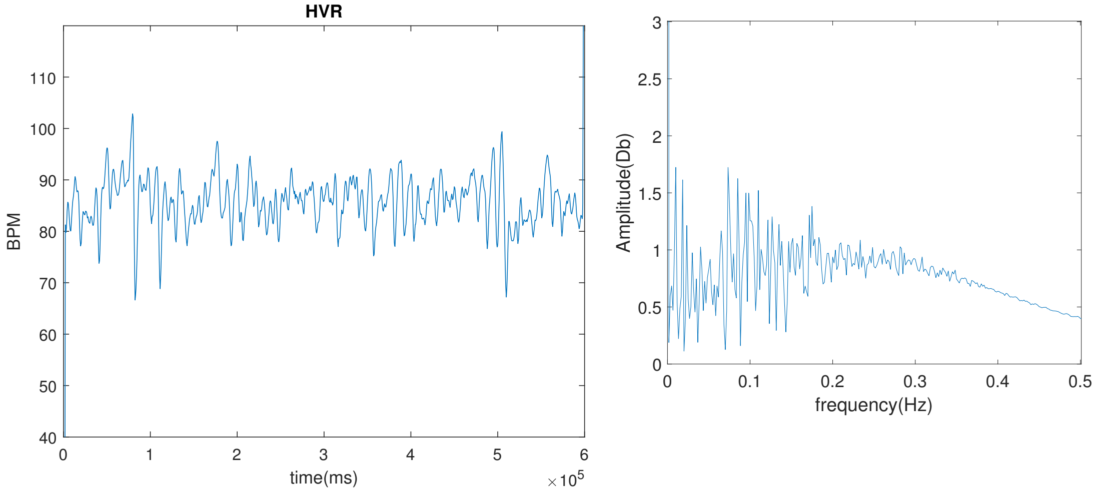

(a) Heart rate

(b) HRV power spectrum

Figure 4.29: HRV subject 5

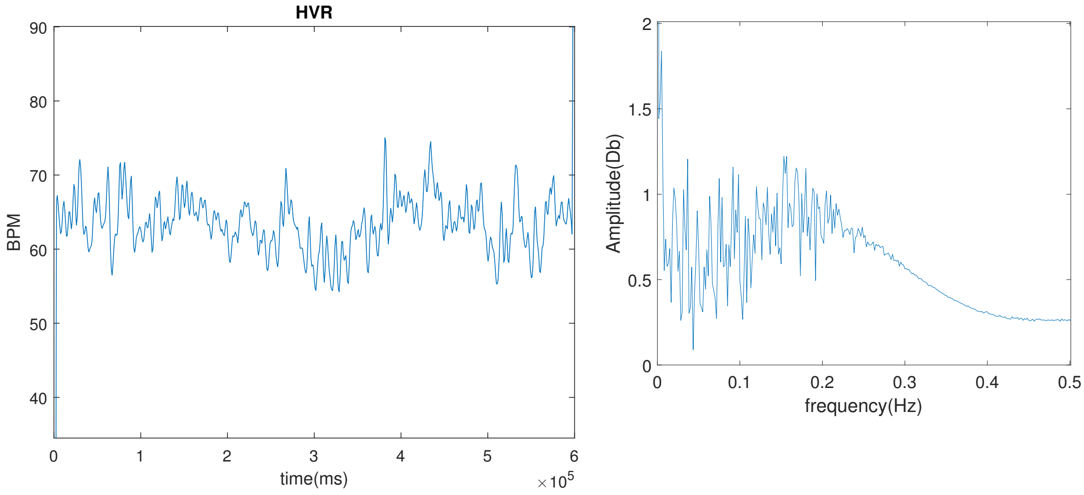

(a) Heart rate

(b) HRV power spectrum

Figure 4.30: HRV subject 6

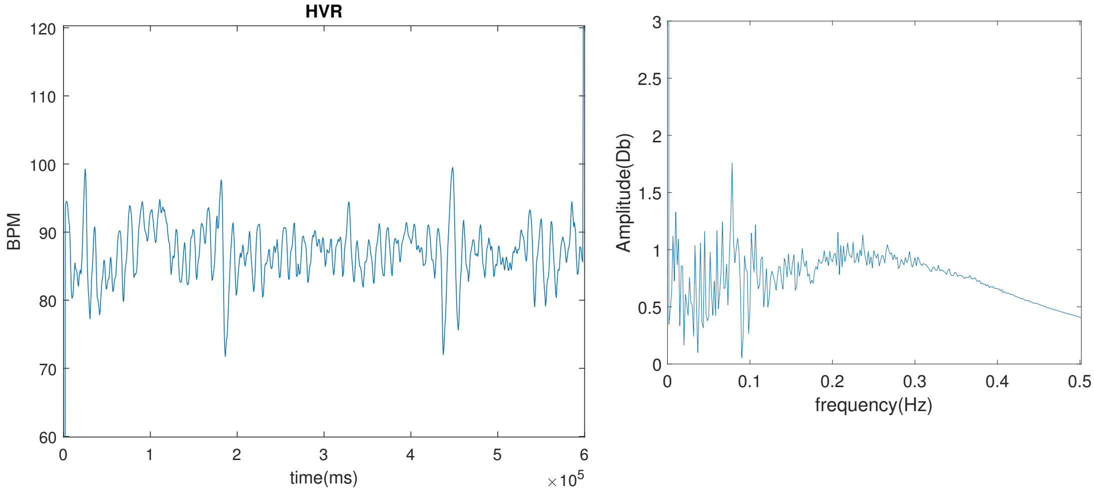

(a) Heart rate

(b) HRV power spectrum

Figure 4.31: HRV subject 7

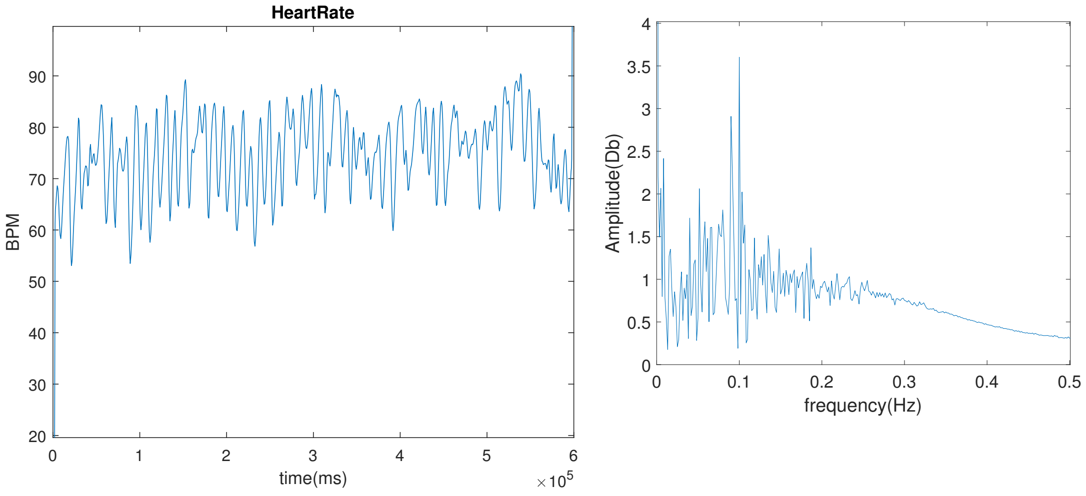

(a) Heart rate

(b) HRV power spectrum

Chapter 5

Future work and Conclusion

5.1 Future Work

Most of the work done in this master thesis has been reaffirming or conforming existing methods on measured raw data from several subjects[1]. However, these methods are all done on a preexisting set of measurements, and a great motivation behind the origin of this thesis is to make these methods work in real time as well. For that to happen, the first step must be real-time filtering of the signal. Luckily, Simulink in Matlab has excellent tools for handling real-time processing of signals, and since the NLMS-algorithm only minimizes the instantaneous cost at each iteration, the processing power needed for real-time implementation should be negligible, as long as care is taken in choosing proper step-sizes. Filtering using instead DWT, as mentioned earlier, will likely be just as effective, and as mentioned in the discussion, has several strengths that make it preferable to an NLMS-filter in a future implementation. Additionally, other studies [15] [27] have approached real-time filtering of ECG from several different angles, granting insight that may further improve the filter. It is worth mentioning, however, that even though Matlab is a powerful tool with excellent handling of large sets of data, it might be worth considering implementing these methods in another language (e.g. Python or C) in order to make it computationally easier on eventual hardware with sparse amounts of power. Next, a real-time implementation of baseline wandering removal shall be attempted. Though this is also a form of filtering the signal, it will be most likely be slightly harder than straight-forward high-frequency filtering. This is due to the need for a posteriori knowledge about trends in the signal, at least for any implementation

---

[1] With the notable exception of the signal separation algorithm, which is to the author's knowledge is a not yet attempted method for ECG-signal processing

using polynomial splines (such as LOESS) or moving averages, making the processing at best pseudo real-time (which is good enough for most practical purposes). Baseline wandering removal using DWT or EMD will probably enhance this performance, and there are in fact papers on pseudo real-time EMD filtering of EEG signals that perform quite well [28], but whether or not this comes at the cost of increased processing power or loss of information remains to be seen. It is nonetheless imperative that any method for baseline wandering removal is able to retain the information removed so it can be further analyzed. The algorithm for QRS-complex detection is, as of now, quite stable, and has performed outstandingly on the measurements used in this thesis. A more extensive testing on a more varied set of data from different subjects is desirable, however, for the sake of confirming the validity of the method in different situations, and an experimental design for this purpose is likely to be made in the future. As for the cycle separation algorithm, some improvements are to be made. First of all, the separation distance should no longer be statically set based on the mean heart rate, but change based on the temporal heart rate at that location in order to both avoid redundant replication of information and avoid failing to encompass all information. If the method shall operate in real-time, the matrix containing these cycles must also be designed in a way as to continuously update its size with respect to the varying sizes of concurrent cycles. Furthermore, and as mentioned earlier, the criteria for artifact classification needs to be better defined. A simple way of doing this could be to combine the existing cross-correlating method with some other approach that would more precisely classify cycles. Also, more multivariate analysis should be done on the cycles with methods such as e.g. Principal Component Analysis(PCA) and Partial Least Square Regression(PLSR). Such analysis might give information about physiological phenomena based on the variance between cycles, and would be of utmost interest. Lastly, more work should be done on determining the respiratory movement in the signal. The most critical part of this stage would be to set up an experimental design, in which the subjects would be equipped with an respiratory belt, and instructed to breathe in a certain pattern underway in the measurement. Thus, it would be possible, with a much higher degree of accuracy, to say whether or not the methods used in this thesis are adequate. An investigation should also be done on whether or not the EDR is a signal possible to identify from the aforementioned heart cycle variance. Any work beyond that other than refining what's already done, would likely be to look for signs of other physiological phenomena not typically considered in ECG-signals. One could also perhaps extend the part of the methods to other bodily signals such as, for example, EEG.

5.2 Conclusion

A set of methods was created for pre-processing the ECG-signals with respect to frequency content and signal morphology, and a rudimentary framework was laid for further multivariate analysis. An NLMS-filter was created and implemented for filtering out high-frequency noise and power line interference. The filter performed well in minimizing the error between the input signal and given reference signal, but some slight distortions in the signal morphology was detected when the signal entered highly stochastic environments, and for future implementations, another approach will be used. The three different methods for estimating the baseline wandering all showed good results, but the EMD method showed a distinctly poorer performance compared to the Savitzky-Golay filter and the DWT. The Savitzky-Golay filter also changed the signal morphology slightly, and so, the DWT estimated baseline was shown to represent the baseline wandering most accurately out of the three methods. The method for identifying QRS-complexes was successfully implemented using a DWT, and proved to be highly accurate in all seven subjects, with only QRS-complexes showing the correct morphology being correctly detected. The algorithm for separating the signal into separate heart cycles performed as desired, and the first part of the artifact classification successfully extracted the premature ventricular heartbeats whenever they arose. However, cycles from subjects with large differences between high and low temporal heart rate showed a tendency to overlap with each other, and a future implementation will take this into consideration. The second part of the artifact classification also worked markedly well, with reference signals being accurately generated and updated, but the algorithm proved to be overly zealous in the sense that it classified several normal cycles as artifacts, and as such, should be further improved upon. The respiratory rate estimation was rather uncertain due to the lack of a reference respiratory signal, but in the power spectrum of the HRV, frequency content was observed that closely matched what was empirically observed in the subjects. In order to quantify the performance of this estimation method, it was decided that a new estimate will be done at a later date with a proper reference signal.

Bibliography

[1] M.J.E. Golay A. Savitzky. Smoothing and differentiation of data by simplified least squares procedures. *Analytical Chemistry*, 36(8):1627–1639, July 1964.

[2] Paul S. Addison. *The Illustrated Wavelet Transform Handbook - Introductory Theory and Applications in Science, Engineering, Medicine and Finance.* IOP Publishing, 2002.

[3] Paul S. Addison. Wavelet transforms and the ecg: a review. *Physiological measurements*, (28), August 2005.

[4] Wardkein Paramote Anchalee Manosueb, Koseeyaporn Jeerasuda. Pli cancellation in ecg signal based on adaptive filter by using wiener-hopf equation for providing initial condition. *Computational and Mathematical Methods in Medicine*, July 2014.

[5] Manpreet Kaur Ankit Jayant, tripti Singh. Different techniques to remove baseline wander from ecg signal. *International Journal of Emerging Research in Management and Technology*, 2(6):16–19, June 2013.

[6] J.M. McCool B. Widrow, J.R. Glover. Adaptive noise canceling: Principles and applications. *Proceedings of the IEEE*, 63(12):1692–1716, December 1975.

[7] Bernard Cazelles, Mario Chavez, Guillaume Constantin de Magny, Jean-Francois Guégan, and Simon Hales. Time-dependent spectral analysis of epidemiological time-series with wavelets. *Journal of The Royal Society Interface*, 4(15):625–636, 2007.

[8] R. Deering and J. F. Kaiser. The use of a masking signal to improve empirical mode decomposition. In *Proceedings. (ICASSP '05). IEEE International Conference on Acoustics, Speech, and Signal Processing, 2005.*, volume 4, pages iv/485–iv/488 Vol. 4, March 2005.

[9] S.Berman E.A.Simoes, R.Roark and J.Murphy. Respiratory rate: measurement of variability over time and accuracy at different counting periods. *Arch Dis Child*, October 1991.

[10] Yunchao Gao, Guangtao Ge, Zhengyan Sheng, and Enfang Sang. Analysis and solution to the mode mixing phenomenon in emd. 5:223–227, 06 2008.

[11] Andrea Zoccola George B. Moody, Roger G. Mark and Sara Mantero. Derivation of respiratory signals from multi-lead ecgs. *Computers in Cardiology*, 12:113–116, 1985.

[12] Axel Loewe Walther H. W. Schulze Olaf dössel Gustavo Lenis, Nicolas Pilia. Comparison of baseline wander removal techniques considering the preservation of st changes in the ischemic ecg: A simulation study. *Computational and Mathematical Methods in Medicine*, 2017:13, March 2017.

[13] Simon Haykin. *Neural Networks - A comprehensive foundation*. Prentice hall, 2 edition, 1999. chapter 5, least-mean-square algorithm.

[14] E.Farahabidi A.Farahabadi Hossein Rabbani, M.Parsa Mahjoob. R peak detection in electrocardiogram signal based on an optimal combination of wavelet transform, hilbert transform and adaptive thresholding. *Journal of Medical Signals and Sensors*, 1(2):91–98, May-August 2011.

[15] R. Schmid T. Stovanov R. Abächerli I. Christov, T. Neycheva. Pseudo-real-time low-pass filter in ecg, self-adjustable to the frequency spectra of the waves. *Medical and Biological Engineering and Computing*, 55(9):1579–1588, September 2017.

[16] Sang-Woong Lee & Unsang Park Jeong-Seon Park. R peak detection method using wavelet transform and modified shannon energy envelope. *Journal of Healthcare Engineering*, July 2017.

[17] Chia-Hung Lin. Frequency-domain features for ecg beat discrimination using grey relational analysis-based classifier. *Computers and Mathematics with Applications*, 55(4):68 –690, 2008.

[18] B.H. Larbi M. Merah, T.A. Abdelmalik. R-peaks detection based on stationary wavelet transform. *Computer Methods and Programs in Biomedicine*, 121(3):149–160, October 2015.

[19] Matlab. emd - empirical mode decomposition. "`https://se.mathworks.com/help/signal/ref/emd.html`", March 2018.

[20] Rajesh Mehra Nidhi Rastogi. Analysis of savitzky-golay filter for baseline wander cancellation in ecg using wavelets. *International Journal of Engineering Sciences and Emerging Technologies*, 6(1):15–23, August 2013.

[21] IEEE Nitish V. Thakor, Senior Member and IEEE Yi-Sheng Zhu, Senior Member. Applications of adaptive filtering to ecg analysis: Noise cancellation and arrhythmia detection. *IEEE transactions on biomedical engineering*, 1991.

[22] Steven R. Long Kenneth C. Arnold Xianyao Chen Karin Blank Norden E. Huang, Zhaohua Wu. On instantaneous frequency. *Advances in Adaptive Data Analysis*, 1(2):177–229, April 2009.

[23] Steven R. Long Manli C. Wu Hsing H. Shih Quanan Zheng Nai-Chyuan Yen Chi Chao Tung Henry H. Liu Norden E. Huang, Zheng Sheng. The empirical mode decomposition and the hilbert spectrum for nonlinear and non-stationary time series analysis. *Proceedings of the royal society a*, 454(1971), March 1998.

[24] Zhaohua Wu Norden E. Huang. A review on hilbert-huang transform: Method and its applications to geophysical studies. *Reviews of Geophysics*, 46(2):1–23, June 2008.

[25] Shiv Dutt Joshi Praveen Gupta, Kamalesh Kumar Shamar. Baseline wander removal of electrocardiogram signals using multivariate empirical mode decomposition. *Healthcare Technology Letters*, 6:164–166, November 2017.

[26] William H. Press, Saul A. Teukolsky, William T. Vetterling, and Brian P. Flannery. *Numerical Recipes in FORTRAN; The Art of Scientific Computing*. Cambridge University Press, New York, NY, USA, 2nd edition, 1993.

[27] R. Farina G. Sannino S. Cuomo, G. De Pietro. A revised scheme for real time ecg signal denoising based on recursive filtering. *Biomedical Signal Processing and Control*, 27:134–144, February 2016.

[28] A. Santillán-Guzmán, M. Fischer, U. Heute, and G. Schmidt. Real-time empirical mode decomposition for eeg signal enhancement. In *21st*

European Signal Processing Conference (EUSIPCO 2013), pages 1–5, Sept 2013.

[29] S. Sarkar, S. Bhattacherjee, and S. Pal. Extraction of respiration signal from ecg for respiratory rate estimation. In *Michael Faraday IET International Summit 2015*, pages 336–340, Sept 2015.

[30] William T. Vetterling Brian P. Flannery Saul Teukolsky, William H. Press. *Numerical Recipes in C: The Art of Scientific Computing.* Cambridge University Press New York, 2 edition, 1992.

[31] Dr. M. K. Soni Seema Nayak and Dr. Dipali Bansal. Filtering techniques for ecg signal processing. *IJREAS*, 2012.

[32] Sharma K.K. Sharma H. Baseline wander removal of ecg signals using hilbert vibration decomposition. *Electronics Letters*, 6(51):447–449, 2015.

[33] M. E. Torres, M. A. Colominas, G. Schlotthauer, and P. Flandrin. A complete ensemble empirical mode decomposition with adaptive noise. In *2011 IEEE International Conference on Acoustics, Speech and Signal Processing (ICASSP)*, pages 4144–4147, May 2011.

[34] Davis University of California. Introduction to digital filters. "`http://123.physics.ucdavis.edu/week_5_files/filters/digital_filter.pdf`", 2013.

[35] Viktor. Introduction to the empirical mode decomposition method. "`https://www.mql5.com/en/articles/439`", June 2012.

[36] Gang Wang, Xianyao Chen, Fang-Li Qiao, Zhaohua Wu, and Norden Huang. On intrinsic mode function. 2:277–293, 07 2010.

[37] Norbert Wiener. *Extrapolation, Interpolation, and Smoothing of Stationary Time Series.* Wiley, 1949.

[38] Lippincott William & Wilkins. *ECG made extremely simple.* Wolters Kluwer, 2011.

[39] Shuen-De Wu, Jin-Chern Chiou, and E. Goldman. Solution for mode mixing phenomenon of the empirical mode decomposition. In *2010 3rd International Conference on Advanced Computer Theory and Engineering(ICACTE)*, volume 2, pages V2–500–V2–504, Aug 2010.

[40] Kobra Zarei, Morteza Atabati, and Malihe Ebrahimi. Quantitative structure-property relationship study of the solvent polarity using wavelet neural networks. 23:937–42, 09 2007.

Appendices

Matlab Code

Main Function

```
%% Parameters

ECGdata = data(1:600000); %10 minute of measurements
Ts = 1000; %Sampling frequency
t = 1:floor(length(ECGdata)/Ts)*Ts; %time in ms



%% Filtering and Baseline estimation

[ECGdata,error,weights] = NLMSfilt50Hz(ECGdata,Ts); % NLMS filtering of high-frequency noise.

sgolBaseline = sgolayfilt(ECGdata,3,4501); %Baseline estimation using Savitzky-Golay smoothing filter.

[filteredECG,dwtBaseline] = ECGwavefilt(ECGdata); % Estimation and extraction of baseline using DWT

imf = EMD(ECGdata); %Empirical mode decomposition of the data
emdBaseline = imf{end}+imf{end-1}+imf{end-2}+imf{end-3}+imf{end-4}+imf{end-5}; %Baseline estiamtion using IMFs



%% Signal component detection

[peaks,R_loc] = locate_R(filteredECG); %Locates the R-peaks in the signal in addition to their amplitudes


%% Heartrate and R-wave amplitude

[heartRate,meanHeartRate] = HRdetection(R_loc,Ts); % Find both the temporal and mean heart rate.
```

```
CurrentHeartRate = reSamp(heartRate,length(t),length(heartRate)); %Extrapolate the heart rate to the same length as the ECG-signal.

R_amp = filteredECG(R_loc); %Amplitude of R-peaks
currentR_amp = reSamp(R_amp,length(t),length(R_amp)); %Extrapolate the R-amplitude to the same length as the ECG-signal.




%% Signal separation

[s,a] = EKGsep(filteredECG,meanHeartRate,Ts); %Separate the ECG-signal into Samples and artifacts.
s(1:5,:) = []; %Remove the first 5 samples.
s(end-5:end,:) = []; %Remove the last 5 samples.
s(~any(s,2),:) = []; %Removes empty sample if any.
[samples,artifacts] = sortSamples(s,a); % Separates any further artifacts from the samples



%% Generating reference cycle

C = 2; %Number of PCA components

Z = Zref(samples); %extract the mean signal of the samples
normZ = normalizeZ(samples,Z); %Translation of samples to mean sample
[U,S,V] = svd(samples,0);

P = V(:,1:C); %Extract loadings from right singular values

percExp1 = S(1,1)/sum(diag(S)); %explained variance of the first two loadings
percExp2 = S(2,2)/sum(diag(S));

```

```
%% plots

figure(1)
subplot(3,1,1)
plot(t,filteredECG);
hold on
plot(R_loc,filteredECG(R_loc),'ro');
hold off
title('Detected R-peaks');
xlabel('time(ms)');
ylabel('voltage(V)');

subplot(3,1,2)
plot(t,CurrentHeartRate);
title('HeartRate');
xlabel('time(ms)');
ylabel('BPM');

subplot(3,1,3)
plot(t,currentR_amp);
title('splined R-amplitude');
xlabel('time(ms)');
ylabel('voltage(V)');



figure(2)
subplot(3,1,1)
plot(t,ECGdata,t,sgolBaseline);
title('S-G estimated baseline');
xlabel('time(ms)');
ylabel('voltage(V)');

subplot(3,1,2)
plot(t,ECGdata,t,dwtBaseline);
title('DWT estimated baseline');
xlabel('time(ms)');
ylabel('Voltage');

```

```
subplot(3,1,3)
plot(t,ECGdata,t,emdBaseline);
title('EMD estimated baseline');
xlabel('time(ms)');
ylabel('voltage(V)');



figure(3)
hold on;
plot(initialRefSample);plot(endRefSample)
title('Initial and final reference sample')
xlabel('time(ms)')
ylabel('voltage(V)')
legend('Initial reference','Final reference')


plotCycles(samples,'samples');
plotCycles(artifacts,'artifacts');


figure(6)
subplot(C,1,1)
p1 = P(:,1)';
plot(p1);
title('Loading 1')
legend(strcat('explained variance = ', num2str(percExp1)));

subplot(C,1,2)
p2 = P(:,2)';
plot(p2);
title('Loading 2')
legend(strcat('explained variance = ',num2str(percExp2)));
```

NLMS filter

```
function [y,error,w] = NLMSfilt50Hz(data,Ts)

%This function uses an adaptive normalized least mean
```

```
    square filter in
%order to remove almost all frequencies above
    approximately 40Hz. Some PLI
%still remains, but is about 3 order of magnitudes
    smaller than the actual
%signal, which is for the most part negligable. If the
    measurement is done
%on a power line using 60Hz, change the sigFC variable
    accordingly.

FrameSize = 1000;
NumIter = floor(length(data)/FrameSize);
Nyquist = Ts/2;
filtLength = 128;
step = 0.01;
filtOrder = 200;
filtFc = 40; %The cutoff frequency of the desired
    filter signal.
sinAmp = 0.0001; %Amplitude of the added sine noise.
sigFc = 50; %Known PLI frequency. Change to 60 if the
    region calls for it.

lmsFilt = dsp.LMSFilter('Length',filtLength,'Method','
    Normalized LMS','StepSize',step,'AdaptInputPort',
    true);
firFilt = dsp.FIRFilter('Numerator',fir1(filtOrder,
    filtFc/Nyquist));
sine = dsp.SineWave('Amplitude',sinAmp,'Frequency',
    sigFc,'SampleRate',1,'SamplesPerFrame',FrameSize);

%freqz(firFilt);

TS = dsp.TimeScope('TimeSpan',FrameSize*NumIter,'
    TimeUnits','Seconds',...
     'YLimits',[-0.0015 0.0015],'BufferLength',2*
        FrameSize*NumIter, ...
     'ShowLegend',true,'ChannelNames', ...
     {'Noisy signal', 'Filtered signal'});

s = zeros(FrameSize*NumIter,1);
error = zeros(FrameSize*NumIter,1);
```

```

for k = 1:NumIter
    x = data((k-1)*FrameSize+1:k*FrameSize)';
    d = firFilt(x);% + sine();
    [y,e,w] = lmsFilt(x,d,1);
    TS([d,e]);
    s((k-1)*FrameSize+1:k*FrameSize,1) = y;
    error((k-1)*FrameSize+1:k*FrameSize,1) = e;
end

y = s';

end
```

ECG baseline estimation

```
function [filteredECG,bl] = ECGwavefilt(data)

%This function takes in an ECG-signal, and decomposes it into 'waveLev'
%distinct detail coefficients. A baseline is estimated by adding detail
%coefficients from 'waveLev' to 'waveLev-filtLev', and is iteratively and
%algebraically removed from the signal.

waveLev = 12;
filtLev = 2;


wt = modwt(data,waveLev);
mra = modwtmra(wt);
assignin('base','mra',mra);

filteredECG = data;
baseline = mra(end,:);
bl = zeros(size(data));

for k=1:filtLev
     filteredECG = filteredECG-baseline;
     baseline = mra(end-k,:);
```

```
    bl = bl + baseline;
end

filteredECG = filteredECG-baseline;

end
```

Empirical Mode Decomposition

```
function [imf] = EMD(data)

%Credit goes to Alan Tan, who is the original creator of this
%EMD implementation.

data = transpose(data(:));
N = length(data);
n =1;
imf = [];

while ~ismonotonic(data)

    x1 = data;
    sd = Inf;

    while (sd > 1)

        [~, upperLocs] = findpeaks(x1); %find the max and minimum points of the curve
        [~, lowerLocs] = findpeaks(-x1);

        uSpline = spline([0 upperLocs N+1],[0 x1(upperLocs) 0],0:N); %Create a cubic spline for respectively the max and min points
        lSpline = spline([0 lowerLocs N+1],[0 x1(lowerLocs) 0],0:N);
        x2 = x1 - (uSpline(1,2:end) + lSpline(1,2:end))/2;

        sd = sum((x1 - x2).^2)/sum(x1.^2);

```

```
            x1 = x2;
            n = n+1;

        end

        imf{end+1} = x1;
        data = data - x1;
end

imf{end+1} = data;

end
```

Detection of QRS-complexes

```
function [peaks,R_loc] = locate_R(data)

wt = modwt(data,10);
mra = modwtmra(wt);

[peaks,R_loc] = findpeaks(mra(5,:),'MinPeakProminence'
    ,1.0*10^(-4),'MinPeakDistance',200);


end
```

Heart rate detection

```
function [heartRate,meanHeartRate] = HRdetection(R_loc,
    Ts)

%Detects the heart rate as the time over three
    consecutive R_loc values divided
%by the sampling frequency Ts. Also returns the mean
    heart rate over the
%whole aray R_loc.

TbP = zeros(1,length(R_loc)); %Time (in ms) between R-
    peaks

heartRate = [];

```

```
for k = 1:length(R_loc)
    if (k+1<length(R_loc))
        TbP(k) = R_loc(k+1) - R_loc(k);
    end
    if k>3
        heartRate(k) = 60/(sum(TbP(k-2:k))/(3*Ts));
    end
end

meanHeartRate = 60/(sum(TbP)/(length(TbP)*Ts));

end
```

Resampling

```
function [y] = reSamp(data,heartRate,refHeartRate)

%Resamples the data to a new size based of the ratio between the integer
%values heartRate and refHeartRate. If the ratio is larger than one, that
%data is extrapolated, and if it is smaller than one, it is interpolated.


beatRatio = heartRate/refHeartRate;
extendedTime = 1:ceil(length(data)*beatRatio);

newDataPoints = 1:beatRatio:length(extendedTime);

if beatRatio >= 1
    resampledData = interp1(newDataPoints,data,extendedTime,'linear','extrap');
else
    resampledData = interp1(data,extendedTime);
end

y = resampledData;

end
```

ECG cycle separation

```
function [s,a] = EKGsep(data,refHeartRate,Ts)

%Separates the signal into seaparate cycles and artifacts. The separation
%happens a distance of 'sepDist' samples from the R-peak at either side, and
%adapts to the value of 'refHeartRate'. If the time between detected
%R-peaks exceeds a certain value based on the 'missHeartThreshold', the
%data between the R-peaks will be classified as an artifact.

missHeartThreshold = 1.5; %Threshold value for artifact classification

sepDist = round(((60/refHeartRate)*Ts)/2); %the seperation distance from the R-peaks
[~,R] = locate_R(data);

s = zeros(length(R),sepDist*2+1);
a = [];

timeBetweenR = diff(R);
c = 0;

for k = 1:length(R)-1
    if (R(k)-sepDist >= 0)&&(R(k)+sepDist <= length(data))
        s(k,:) = data(R(k)-sepDist:R(k)+sepDist);
        if ((timeBetweenR(k)>missHeartThreshold*(2*sepDist))&&(k>2)) %Classifies sample as artifact if no QRS-complex is detected after a certain time.
            c = c+1;
            a(c,:) = data(round(R(k)-(R(k)-R(k-1))/2)-sepDist:round(R(k)-(R(k)-R(k-1))/2)+sepDist);
        end
```

```
    end
end

end
```

Cycle classification

```
function [samples,artifacts] = sortSamples(unsortedSamples,anomalySamples)

%take the first 10 heartBeats in unsortedSamples, and use as a reference
%the mean of them. For every heartbeat in unsortedSamples, check then the
%normalized cross-correlation between the heartbeat and the reference
%heartbeat. If the crosscorrelation at any point peaks over the set
%corrThreshHold, it passes and is sorted into samples, and the reference
%beat is updated by taking a new mean of this new sample together with the
%previous ones. Else, its form deviates from what is deemed "normal",
%and it will be sorted into artifacts for later analysis

corrThreshHold = 0.97;

refSample = Zref(unsortedSamples(40:60,:)');
assignin('base','initialRefSample',refSample);

samples = [];
artifacts = [];
c = 0;


for k = 1:length(unsortedSamples(:,1))
    sampleCorr = xcorr(refSample,unsortedSamples(k,:),'coeff');

```

```
    %plot(refSample);

    if max(sampleCorr) > corrThreshHold
        samples(k-c,:) = unsortedSamples(k,:);
        refSample = Zref(samples');
        %disp(k);
    elseif max(sampleCorr) < corrThreshHold
        c = c + 1;
        artifacts(c,:) = unsortedSamples(k,:);
        %disp(k);
    else
        disp('something something');
    end
end

assignin('base','endRefSample',refSample);

artifacts = [artifacts; anomalySamples];
```

Reference cycle creation

```
function [z] = Zref(samples)
%Takes in an matrix 'samples', and outputs a an array that is the mean
%values of all the columns in 'samples'.

z = zeros(1,length(samples(:,1)));

for k = 1:length(samples(:,1))
    z(k) = mean(samples(k,:));
end

end
```